A LIQUID CRYSTAL BASED

ELECTRON SHOWER DETECTOR

by

RAYMOND ADKINS

Submitted in partial fulfillment of the requirements

For the degree of Masters of Science

Department of Physics

CASE WESTERN RESERVE UNIVERSITY

May, 2018

CASE WESTERN RESERVE UNIVERSITY

SCHOOL OF GRADUATE STUDIES

We hereby approve the thesis/dissertation of

Raymond Adkins

candidate for the degree of Masters of Science *.

Committee Chair

Dr. Charles Rosenblatt

Committee Member

Dr. Rolfe Petschek

Committee Member

Dr. Benjamin Monreal

Date of Defense

3/27/18

*We also certify that written approval has been obtained

for any proprietary material contained therein.

TABLE OF CONTENTS

LIST OF TABLES

Table Page Number

LIST OF FIGURES

Figure Page Number

A Liquid Crystal Based Electron Shower Detector

Abstract

by

RAYMOND ADKINS

There are numerous applications of liquid crystals spanning many fields of technology. There are also many applications for detecting patterns of ionizing radiation such as X-rays. This project involves using well known properties of liquid crystals to design a detector to display two dimensional patterns of ionizing radiation. Polymerized liquid crystal films were fabricated with one surface being a transparent electrical conductor, and the other open to air. These films were designed so that an optical change in the layers occurs when charged particles are deposited on the surface. This allows for the creation of displays that show the spatial arrangement of deposited charges. It is well known that a gas with appropriate electrical fields can convert patterns of ionizing radiation into patterns of charge. We have explored different liquid crystal and polyimide combinations to create stable hybrid aligned and homeotropically aligned open cells. We have developed an electron source which generated the electrons needed to test the liquid crystal layers. Finally, we have done several tests to better understand the mechanism for inducing a transition in the layers, and to make the liquid crystal films more useful for charged particle detection.

Chapter 1

Introduction

Spatially resolved detection of radiation has many important commercial and scientific applications. The use of x-ray detection ranges from medical purposes to customs enforcement screenings. All of these applications require both a source of X-ray emission, and a sensor to read out the location and relative intensity of the X-rays that in turn report the patterns of high atomic number atoms in objects between the source and the detector. Current methods of X-ray detection often require unwieldy detectors, which are expensive to build in large arrays and are not easily portable for field operations. X-rays are, of course, not the only form of ionizing radiation that may be useful to detect. Detecting the paths of high energy primary and secondary ionizing radiation is a routine need experiments in high energy physics.

In many radiation detection methods, it is common to amplify incoming radiation using a drift region. This region consists of a gas bounded by parallel sheets of conducting mesh that have an applied potential difference to set up an electric field across the region. Incoming ionizing radiation collides with the gas, which results in the generation of electrons. These electrons are then accelerated by the electric field. If the electric field, pressure of the gas and species of the gas have been chosen correctly, these electrons will gain enough energy in their free motion between collisions to produce further ionization event in later collisions. This creates a shower of electrons, which has been amplified from a single ionization event. The goal of this project is to use the well understood physics of liquid crystal displays and electron multiplication, with some important modifications, to create a novel liquid-crystal-based ionizing radiation detector.

Many known liquid crystal displays change patterns of voltage into patterns of light. These work because an electric field applied to a liquid crystal can change its orientation and so its birefringence. This change in birefringence changes the polarization of light and, with appropriate polarizers, results in changes in light patterns. Most liquid crystal displays are made by coating the surface of transparent electrodes with an alignment layer and filling the space between these two electrodes with a liquid crystal. The alignment layers determine the birefringence of the liquid crystal. There are two common modes of alignment; homeotropic and planar. Homeotropic samples are aligned so that the director of the molecules is perpendicular to the interface of the electrodes. Planar samples are aligned so that the liquid crystal molecules are aligned parallel to the plane of the electrodes. By applying a potential difference to the two electrodes, an electric field can be set up across the liquid crystal layer. Due to the dielectric anisotropy of the liquid crystals, this potential difference will cause the director of the liquid crystal to be reoriented.

The samples which we have developed consist of thin layers of liquid crystals that have been deposited onto one transparent conductor. The other boundary is open to air, unlike most other liquid crystal displays, which are bounded on both sides by conductors. In the course of the project, we have developed both homeotropic and hybrid open cells. The open interface requires the samples to be polymerized, so that the thin liquid crystal layers are stable. Having one surface open to the air allows the liquid crystal to act as an ionizing radiation detector by allowing for the deposition of charges on the surface. If the liquid crystal layer is placed under the drift region, the electrons generated in the ionization event will be deposited on the liquid crystal layer. If the bottom electrode is grounded, this will set up a potential across the liquid crystal layer, and will cause the same effect as was described above. The homeotropic cell has

no in-plane birefringence and a negative dielectric anisotropy so the electric field will cause a birefringence as the electric field will cause the liquid crystal to be perpendicular to the field. The hybrid cell has in-plane birefringence and the homeotropic film has no in-plane birefringence. The hybrid cell is composed of a positive dielectric constant liquid crystal that tends to align along an electric field so that an electric field will decrease the birefringence. The homeotropic cell is composed of a liquid crystal that tends to align perpendicular to an electric field so that the electric field tends to increase the birefringence. This birefringence, finally, can be visualized by illuminating the film with polarized light at an angle to the principle directions thereof and observing it through a polarizer at right angles to this polarization. In the absence of birefringence, no light goes through: birefringence, and thus an optical retardation that is not an integer multiple of 2π, will allow light to pass through. In this way, the liquid crystal allows the patterns of charge to be visualized.

To summarize, incoming ionizing radiation will cause an ionization event in the drift region. This ionization event will be amplified to generate a swarm of electrons in the drift region of the detector, which will then be deposited as a 2D charge density on the liquid crystal layer. This will set up a potential difference across the liquid crystal layer, which will cause the liquid crystal molecules to reorient. This will create an optical change in the liquid crystal layers, which can be measured using standard optical equipment. Further development of the project will determine if the liquid crystal layers we have made will be able to allow for the visualization of these 2D charge patterns reliably and more cheaply than standard apparatus.

Chapter 2

Background

This chapter will serve as a brief introduction to the basic physics which will be required to understand the project. This will include a description of liquid crystals and some of their important properties. It will also explore the physics behind the electron sources used to test the layers. Descriptions of the materials and apparatuses specific to this project will be reserved for later chapters.

2.1 Introduction to Liquid Crystals

Liquid crystals were discovered in the late 19th century[1], and have since found use in a diverse range of technological applications[2]. Liquid crystals are phases of matter which possess long range orientational order, like a crystal, but whose individual molecules can flow past one another, like a liquid. In addition to this, liquid crystals have many interesting and important properties. Liquid crystals have several phases which correspond to different degrees of molecular order. In this project, we will limit our focus to liquid crystals in the nematic phase. Nematic liquid crystals have long range orientational order, meaning that the long axis of neighboring molecules align, but do not have a positional order. A cartoon model of this is shown in figure 1. The chemical structure of one of the liquid crystals used in this project is shown in figure 2.

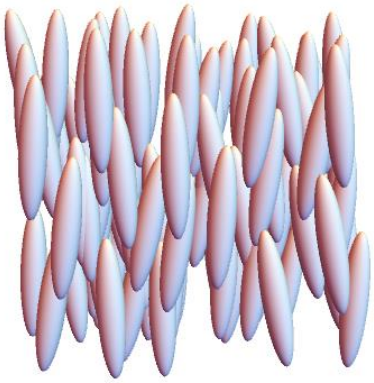

Figure 1: A simplified model of nematic liquid crystals. Each molecule is represented as a cigar shaped object.

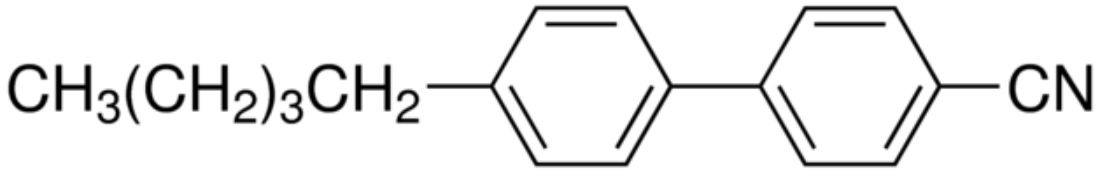

Figure 2: The molecular structure of the liquid crystal 5CB[3].

In this project, several important properties of liquid crystals will be exploited. Liquid crystals are birefringent, meaning that light incident on a liquid crystal film will encounter an index of refraction which is dependent on its polarization. In a uniaxial material, the index of refraction along one axis, the optical axis, has a value n_e and the index of refraction orthogonal to this is n_o where $n_o \neq n_e$. In a birefringent medium, the polarization of the incoming light can be described as a superposition of two light rays. These two orthogonal rays are called the ordinary and the extraordinary rays. The ordinary ray is the component of the light with its polarization perpendicular to the optical axis of the material. The extraordinary ray is the component of the polarization which is parallel to the optical axis of the material. The differing indices of refraction that these two rays encounter causes them to propagate through the material at differing speeds. Because of this, when these two rays recombine upon exiting the liquid

crystal, the polarization of the light may be changed. Most generally speaking, incoming linearly polarized light will exit the material with an elliptical polarization, as long as the incoming light is not polarized along one of the eigenvectors.

Liquid crystals also have a dielectric anisotropy, meaning that their dielectric permeability is dependent on the orientation of the liquid crystal molecules in the bulk[4]. This may be due to a dipole moment or induced dipole in the molecular structure of the liquid crystal. These microscopic details will not be our focus, as they have been explored. We will only be interested in the macroscopic effects of the dielectric anisotropy which will be used to design the electron detector. The dielectric anisotropy leads to an energetically favored orientation of the liquid crystal molecules when immersed in an external electric field. If the long axis of the liquid crystal molecule, called the director, aligns with the applied electric field, the liquid crystal is said to have a positive dielectric anisotropy. If the director of the liquid crystal aligns perpendicular to the applied electric field, the liquid crystal is said to have a negative dielectric anisotropy. Birefringence and dielectric anisotropy are the basic physics which have underpinned liquid crystal devices for decades.

Liquid crystal are often aligned in two different ways; homeotropically and planar. When a liquid crystal is aligned with its director perpendicular to an interface, it is said to be homotopically aligned. When a liquid crystal is aligned with its director parallel to the interface, it is said to have planar alignment. There is also a third possibility, which will be important in this project. When a liquid crystal has one boundary having homeotropic alignment and the opposite boundary having planar alignment, it is said to have hybrid alignment. The alignment of the liquid crystal is important when determining the optical properties of the liquid crystal cell. When a liquid crystal is aligned homeotropically, it is no longer birefringent to light propagating

along the director, since the liquid crystal now has rotational symmetry about the propagation axis of the light[5]. When the liquid crystal is planar or hybrid aligned, this symmetry is broken, and the layer is birefringent.

When making liquid crystal displays, it is common to arrange liquid crystals that have a negative dielectric anisotropy in a homeotropic alignment, and to arrange liquid crystals that have a positive dielectric anisotropy in a planar or hybrid alignment. In these orientations, a change in directional order can be induced by applying an electric field perpendicular to the plane of the liquid crystal layer. This change in directional order will act as a switch to turn on or off the birefringence of the liquid crystal layers. When observed under crossed polarizers this will clearly be visible. When the layer is homeotropic, and therefore not birefringent, no light will pass through the crossed polarizers, leading to a dark state. When the layer is planar or hybrid aligned, the liquid crystal is birefringent and the polarization of the light will change when passing through the liquid crystal layer. This will allow some light to pass through the top polarizer, which will lead to a bright state.

The initial alignment of a liquid crystal layer is often done by coating a glass surface with a polyimide layer. A polyimide is a polymer with its repeating monomers linked by an imido group, as shown in figure 3. The interaction of the liquid crystal with the polyimide layer imposes orientational boundary conditions on the liquid crystal, which affects the orientation of the director throughout the cell. There are many different polyimides used to induce both homeotropic and planar alignment, which have been well characterized, and are commonly used in commercial applications.

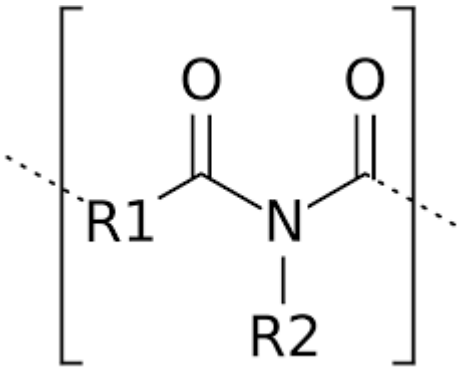

Figure 3: General chemical formula of a polyimide. R is meant to represent the chemical structure specific to each polyimide.

One final important property of liquid crystals is their elasticity. There are several simple geometries in which the nematic molecules are all aligned in roughly the same direction. Any perturbation from this simple alignment will involve deformation of a bend, twist or splay[6]. These three possibilities are shown in figure 4.

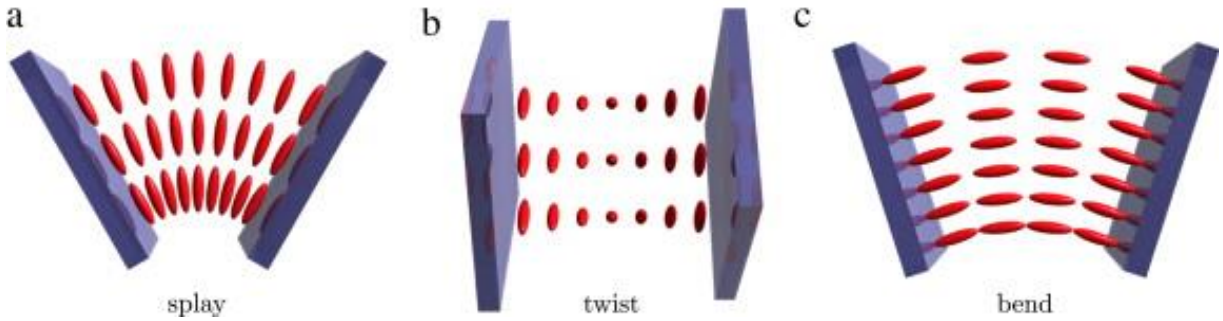

Figure 4: The three eigenmodes of perturbation to a simply aligned liquid crystal; bend, twist and splay[7].

This perturbation may be due to boundary conditions which do not favor simple alignment, as is done in the case of the hybrid aligned cell, or due to a change in the orientation of the molecules through the application of a field. The resistance of a given liquid crystal to deform in these ways can be represented by the elastic tensor. When the liquid crystal is immersed in an electric field, the interplay between the dielectric anisotropy and the elasticity sets the voltage at which the

molecules reorient themselves. In a cell in which all molecules are roughly aligned, this occurs suddenly, once a critical voltage is reached. This critical voltage is called the Freedericksz transition.

The samples used in this project will be open at one interface, and so will necessarily need to be resistant to fluctuations in ambient conditions and to damage. This can be done through polymerization. Polymer stabilized liquid crystals were developed in the 1990's, and have since been used in sensors, actuators and smart windows[8]. To polymerize a liquid crystal, a reactive mesogen, a molecule having two main components; a liquid crystalline group at its core, and a number of polymerizable end groups. In the case of Reactive Mesogen 82 (RM-82), which will be used in this project, there are two such end groups; one at either end of the molecule. In this project, the reactive mesogen molecules will be dispersed in the liquid crystal. The central body of the molecule, being similar in structure to a liquid crystal used, ensures that the reactive mesogen molecules are roughly oriented along the director of the liquid crystal throughout the sample.

When polymerized, the polymerizable tails of neighboring reactive mesogen molecules form a bond with the help of a catalyst. In this project, we used the catalyst Irgacure 651, a commercially available UV curing agent. When exposed to ultraviolet light, this molecule releases free radicals, which bonds two ends of neighboring RM-82 molecules, forming a chain. When many of these molecules are linked, they form long fibrils along the director, locking in the alignment of the liquid crystal layer. The molecular structure of these two molecules is shown in figure 5.

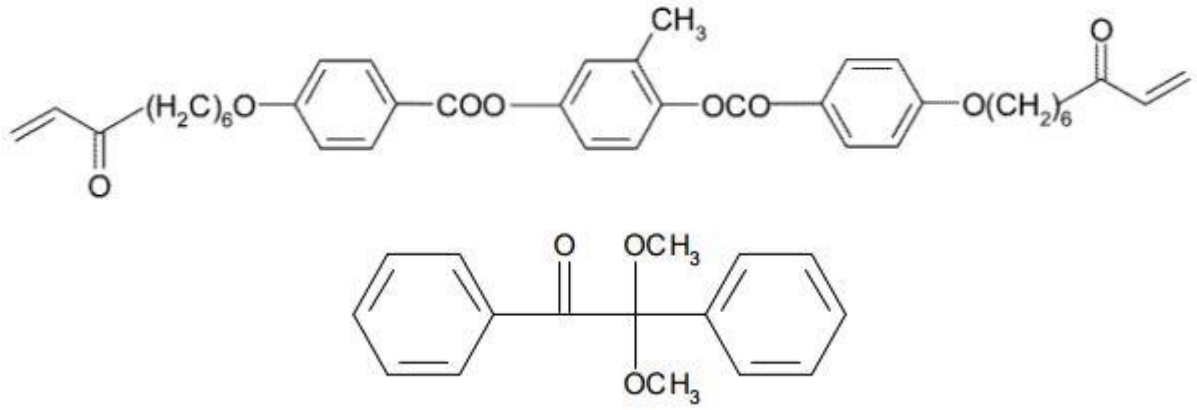

Figure 5: Molecular structures of the RM82[9] (top) and the Irgacure 651[10] (bottom).

The absorption spectrum of the Irgacure is shown below in figure 6. Light with a wavelength of 365 nm was chosen to irradiate the samples, both because it is in the correct region of the spectra to allow for polymerization to occur, and because it is not at the absorption peak of the Irgacure, ensuring that the layers are irradiated more evenly throughout. It is important to note that the polymerization had to take place in an oxygen-free environment. Oxygen inhibits the free radical reaction from polymerizing the RM-82 effectively. In this project, polymerization was done using a lamp of power 0.15 mW cm^{-2} in a blanket of argon. The samples were placed 10 cm away from the lamp.

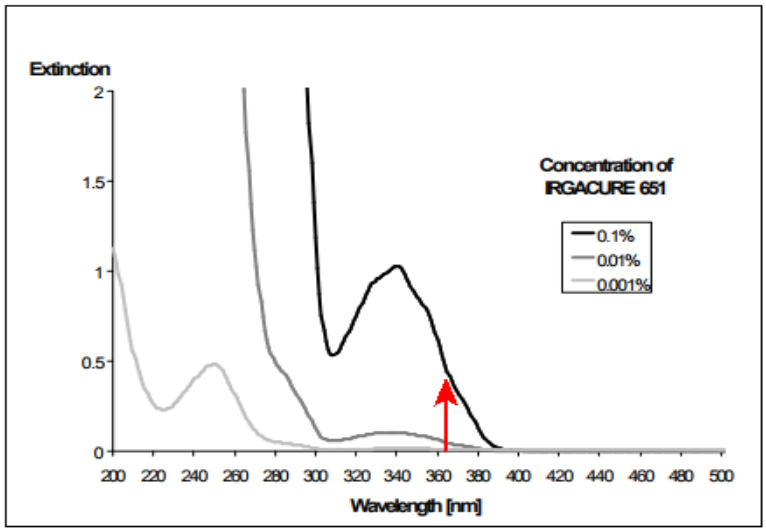

Figure 6: The spectrum of Irgacure, courtesy of the manufacturer's website[11]. The red arrow has been inserted to show the wavelength used to irradiate the samples in this project.

2.2 Introduction to Corona Sources

It is also necessary to understand the properties of a corona electron source. A corona discharge occurs when the gas surrounding a charged conductor is ionized, and begins to carry a current[11]. A corona discharge electron source is made from a charged conductor, often one with a small radius of curvature like a sharpened tip, which is designed to generate and direct this current toward a target held at a lower potential. To create a corona discharge in air, an electric field of tens of thousands of volts per centimeter is required[13]. This is easily achieved by applying a difference of a few thousand volts between a sharpened metal tip and a conducting plate which are spaced a few millimeters apart. Stray electrons or ions from an ambient source will be accelerated to high speeds in this field. At appropriate gas pressures, electric fields and gas used to flood the region, such as argon, it becomes reasonably likely that collisions will produce ionization event. These events will strip electrons off of the gas molecules, further creating electrons. The process is repeated, which can produce a self-sustaining cascade of

electrons and ions which are accelerated away from the sharpened tip[14]. This cascade of electrons and ions is known as a Townsend avalanche, and was discovered in the late 19th century[15]. Depending upon the sign of the voltage applied to the tip, the cascade of particles reaching the target can be either positively or negatively charged. The sign of the applied voltage matches the charge reaching the target, as the ions are repelled from the conducting tip and toward the lower potential plate. For this project we will only be interested in a negative corona discharge.

There are several different regimes of the Townsend avalanche. These regimes typically have sharp transitions, and may be multivalued as a function of applied voltage. The physics of these electron avalanches has been of experimental interest for over a century. Despite this, it is not easy to predict quantitative properties of an electron avalanche for an arbitrary conductor. This is due in part to the many difficult to control variables, such as the shape of the tip and the composition of the gas. Townsend did many of his experiments in the simplest possible geometry: a sealed tube having a flat anode and cathode at either end which was filled with a single species of gas. He found that there are three main regimes as the voltage between the plates is increased, which are shown in figure 7.

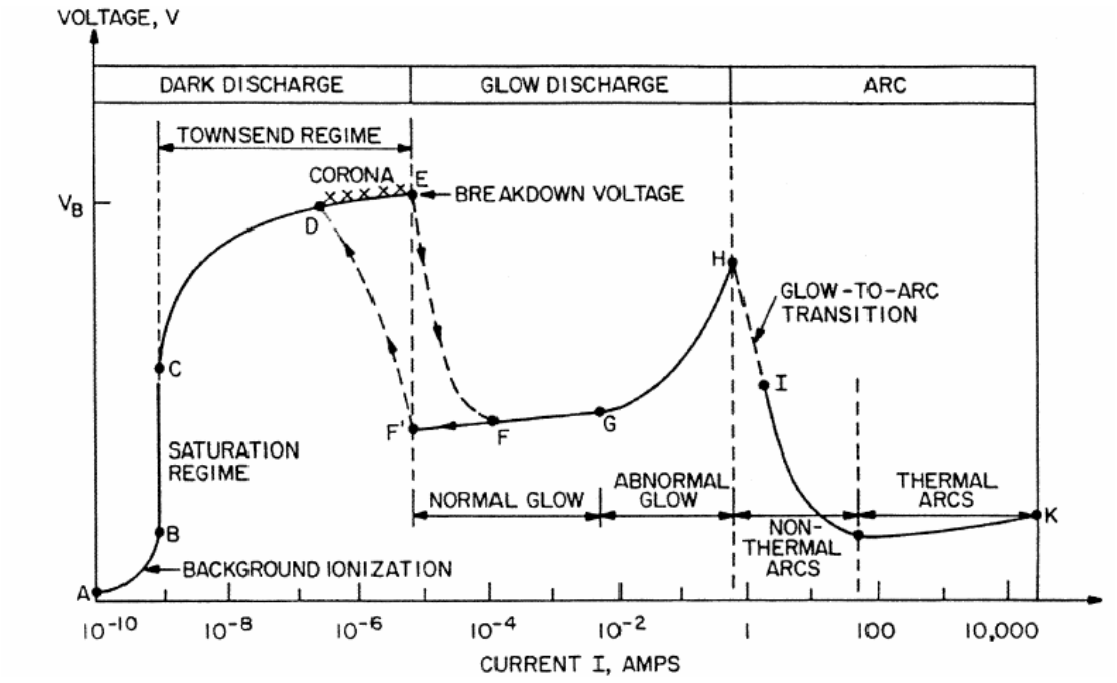

Figure 7: Figure showing the Townsend avalanche for Neon[16]. Note the hysteresis and nonlinear behavior as a function of voltage.

The first is the dark discharge regime, during which the tip does not glow and the current reaching the anode is typically small ($<10^{-6}$ A). Beyond this is the glow discharge regime, where the cathode begins to emit violet and ultraviolet light. This regime will be important, as it will be where the corona source is typically operated throughout this project. As electrons move through the air, they begin to ionize the surrounding gas. As the ions in the gas recombine, they emit light in the violet and ultraviolet range. The glow discharge regime generates a much higher current than the dark discharge regime. The final regime is arcing, which is when the air has broken down, and has a high electrical conductivity. This regime is not useful for our experiment, as it will damage the liquid crystal layers. This regime will be avoided both in this discussion and in experiments.

2.3 Introduction to Gas Electron Multipliers

It is also necessary to understand gas electron multipliers, as their construction and use will be an important goal of the experiment. Gas electron multipliers operate by multiplying a single incoming electron with a gain of several orders of magnitude[17]. This is done in a region of high electric field which is generated by two parallel planes of mesh. The gain is controlled by the magnitude of the electric field in the region. This region is flooded with a gas chosen for use in the multiplier, usually a mixture of a noble gas and some dopant gas. An electron or ion entering this region through the mesh will then collide with the gas in the chamber. This process multiplies the number of electrons, creating a measurable current.

This method of generating electrons has several advantages over a corona source. First, the amount of charge reaching the target can be carefully tuned by measuring the gain of the gas electron multiplier. Secondly, this source will create a thin line of charge which will be deposited on the liquid crystal below. When the alpha particle is emitted, it will travel along a straight path, ionizing the surrounding gas and producing a line of ions. This line will be accelerated downward toward the sample, depositing a thin line of charge on the liquid crystal. The line will be slightly deformed by collisions with the argon, which will be explained further in section 3.8. This will allow for more precise measurement of the spatial resolution of the liquid crystal detector. Finally, it will be a more realistic operating mode than the corona source.

2.4 Electron Shower Detector Overview

The electron shower detector will operate using the similar as a liquid crystal display, with the accompanying changes necessary for this unique application. The layers are designed, as outlined above, to allow for orientational changes when an electric field is applied perpendicular to the liquid crystal layers. This orientational change will change the birefringence of the liquid

crystal layer, which will affect the magnitude of the phase shift (optical retardation) of the polarization of light passing through. When viewed under crossed polarizers, this change in the phase shift will lead to a change of intensity of transmitted light, which then can be detected. One of the key differences from standard liquid crystal displays is the top interface being open to the surrounding gas. The bottom interface is a transparent electrode made of the transparent conductor Indium Tin Oxide, which is coated with a polyimide. This bottom conducting plate is grounded. It is key that the film be open to air at one interface so electrons can be deposited on the surface of the liquid crystal. These charges set up an electric field across the layer, creating an optical pattern on the liquid crystal layer, which mirrors the configuration of the charge distribution on the film. The open surface is the key step in using liquid crystals to detect charged particles, and has required unique fabrication procedures to accomplish.

Liquid crystals with a single free surface have been studied, but are not nearly as common as cells with two solid boundaries. Previous research into open cells has found several liquid crystals which align perpendicular at the air interface[11]. This will be an important factor when choosing the liquid crystal for the electron shower detector. Free surfaces have been important in our lab for interesting studies devoted to topology of liquid crystal films which required open cells[12]. It will also be critical to polymerize the liquid crystal layers to create a more robust film.

Chapter 3

Materials and Methods

This chapter will describe the design and fabrication of materials which will be used in this project. First, we will describe how the liquid crystal samples which were used as electron shower detectors were constructed. Next, we will describe how the corona electron source and the gas electron multiplier were constructed, with important considerations for their use in this project. Finally, we will describe some of the important theoretical considerations for the project and approximations made during the analysis.

3.1 Hybrid Sample Preparation

E7 (Merck) is a commercial mixture of four different liquid crystals having a positive dielectric anisotropy, 51% 4-Cyano-4'-pentylbiphenyl (5CB), 25% 4′-Heptyl-4-biphenylcarbonitrile (7CB), 16% 4'-n-octyl- oxy-4-cyanobiphenyl (80CB) and 8% 4-cyano-4"-n-pentyl-terphenyl (5CT)[1]. This liquid crystal was chosen to make the hybrid aligned samples for the project because of the wide range of temperatures at which it is nematic (-10℃ - 59℃). This ensures that the temperature-dependent properties of the liquid crystal do not change considerably near room temperature due to small temperature fluctuations. The polyimide PI-2555 (Nissan), commonly used to induce planar alignment, was used to coat an ITO slide by spin coating at 3600 rpm for 40 seconds. The samples were then prebaked in an oven at 80°C for 30 minutes, followed by a hard bake at 250°C for 60 minutes. This polyimide was then rubbed unidirectionally with a commercial rubbing cloth. The polyimide backbone induces planar alignment at the bottom interface, and the E7 aligns itself homeotropically at the top interface.

This leads to a hybrid alignment of the liquid crystal, meaning the director of the liquid crystal tilts uniformly from an alignment that is parallel to the bottom glass, to an alignment that is perpendicular to the glass. A diagram of this is shown in figure 8.

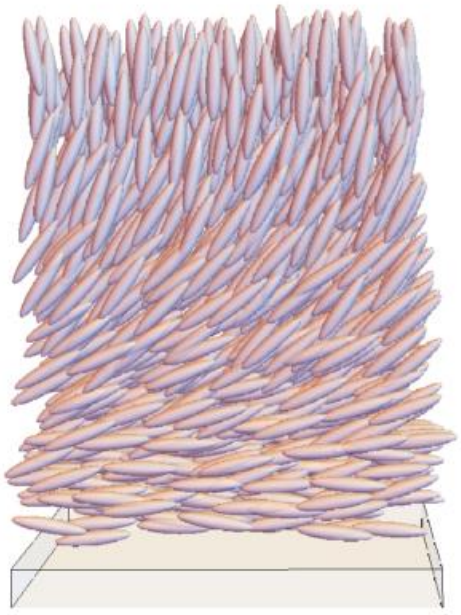

Figure 8: A model of the hybrid cell, showing the orientation of the liquid crystal throughout the cell.

To polymerize the cells, the E7 was doped with a reactive mesogen (RM82) and a Irgacure 651. An ionic polymerization reaction between the RM-82 and the photoinitiator occurs when the sample is exposed to light of wavelength of 365 nm for an extended period of time. This forms a polymer lattice which makes the liquid crystal layers more robust.

3.2 Homeotropic Sample Preparation

The homeotropic samples were much more difficult to prepare than the planar samples. First, the alignment at both the alignment layer-liquid crystal interface and the air-liquid crystal interface needed to be tested. For a given liquid crystal, the alignment at the alignment layer-

liquid crystal interface could be tested by fabricating a closed cell from two slides coated with the alignment layer, and filling the cell with the liquid crystal. If the alignment layer was found to induce homeotropic alignment, alignment at the air-liquid crystal interface was tested by dropping a small amount of the liquid crystal onto a slide coated with the alignment layer. There were several liquid crystals which have a negative dielectric anisotropy which were found to be homeotropic at the air-liquid crystal interface and at the alignment layer-liquid crystal interface. The difficulty in fabricating the layers was mainly due to the wetting of the bottom surface by the liquid crystal. Many homeotropic alignment layers operate by forcing the liquid crystal to minimize its contact with the alignment layer. Minimizing contact between each molecule and the alignment layer means the long axis of the molecules remain perpendicular to the layer. This works well to induce homeotropic alignment, but also means that the liquid crystal does not adhere well to the surface. In closed cells, the liquid crystal is held to the surface of the alignment layer by capillary action, but in open cells this minimization of contact causes the liquid crystal to pull away from the surface, creating unstable alignment.

It was found that the negative dielectric anisotropy liquid crystal mixture ZLI 2806 (Merck) aligns perpendicularly to the air interface, but did not wet the common polyamides used for homeotropic alignment, and did not align homeotropically on several different silane compounds. It was found that it did align well on hexadecyl-trimethyl ammoniumbromide (HTAB), a surfactant which is known to induce homeotropic alignment at glass interfaces. It was found, however, that upon exposing the layers to the corona source, the alignment was damaged. The region which was exposed to the corona source became planar immediately after being used.

It was found that the phospholipid 1,2-Bis(10,12-tricosadiynoyl)-sn-glycero-3-phosphocholine ($DC_{8,9}PC$), was also able to produce homeotropic alignment, and was able to be

effectively polymerized. It was also found that the layers remained stable in the long term. When used under the corona source, the layers were only damaged when repeatedly exposed to a high current. This means that this is not useful as a laboratory grade charged particle detector, but is possible to use for initial tests designed to understand the mechanism of transition in the liquid crystal layers.

To make the homeotropic layers, the ITO was cleaned according to the usual procedure. It was found that the samples could be coated by diluting a small amount of $DC_{8,9}PC$ in ethanol, dropping it onto the surface and letting the ethanol evaporate. The goal was to make a monolayer of the $DC_{8,9}PC$ on the ITO. Several different concentrations of $DC_{8,9}PC$ were diluted in ethanol, and 10 µL of solution were placed on a 2 cm by 2 cm slide. These were then coated with ZLI 2806, and imaged. The results of these tests are shown in figure 9.

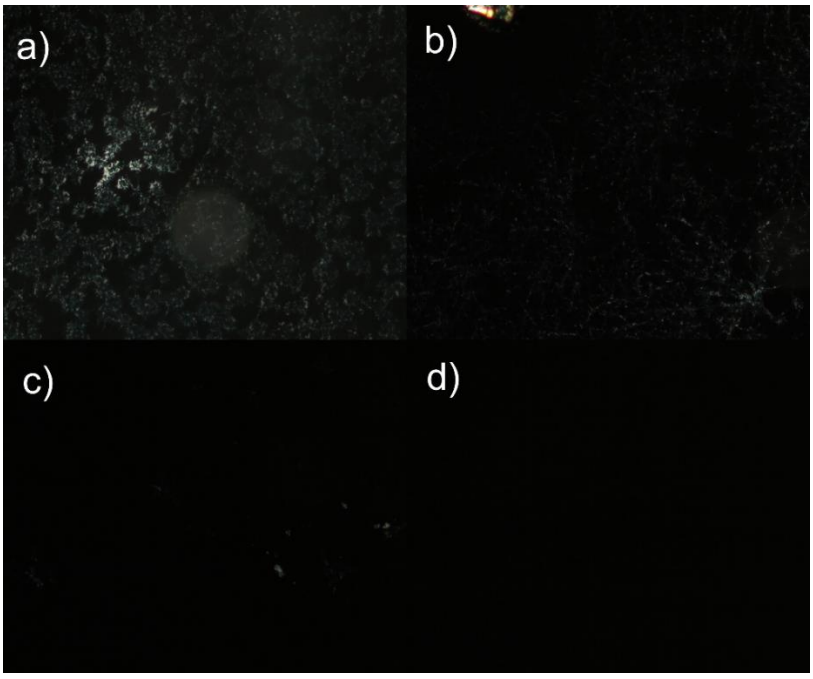

Figure 9: Tests to find the ideal concentration of $DC_{8,9}PC$. The concentrations of the samples in each panel are a) 2 mg/mL b) 1 mg/mL c) 0.25 mg/mL d) 0.05 mg/mL.

It seems that 0.05mg/mL is the right dilution of $DC_{8,9}PC$ in ethanol. It is also important to note that that lowering the concentration to 0.02 mg/mL was found to produce poor alignment. It is believed that when diluted to this level, the monolayer is not completely formed, and therefore does not produce good alignment.

The ZLI 2806 was then diluted to 125 mg/mL. This was then doped with 5 weight percent RM 82 and with 1 weight percent Irgacure 651. 20 µL of the liquid crystal solution was placed on 2 cm by 2 cm slides, and was spin coated at 1700 rpm for 20 seconds.

3.3 Testing the Effectiveness of Polymerization

Although the cells do not need a high degree of polymerization to be used in the detector, they do need a consistent degree of polymerization, so that each detector is identical. To achieve this, it was decided that the cells should be irradiated long enough so that all of the reactive mesogen is polymerized. To ensure that the properties of our polymerized samples do not deviate greatly from the properties of a cell made with pure E7, the minimum amount of RM82 needed for effective polymerization should be used. Previous testing on polymerization found that polymerization was possible at 7% RM82, but not at 3% RM82[2]. My tests have found that 4% RM82 was not enough to allow for full polymerization, but 5% was able to form a polymer.

When polymerization has taken place, the transition temperature from nematic to isotropic is increased. This is because the polymer structure imposes a higher degree of order on the liquid crystal. To find the exposure time needed for total polymerization at 5% RM82 concentration, a single 3cm x 3cm slide was prepared for hybrid alignment as is described in section 2.1, and was then coated with a mixture of E7 with 5 weight percent reactive mesogen. A box made of glass was prepared which was just taller than the liquid crystal coated slide, and was coated with black tape. This effectively blocked the light from reaching the cell. This dark box

was then placed over half of the cell, which was irradiated for 30 minutes. The dark box was then rotated by 90 degrees, and placed over $\frac{2}{3}$ of the cell, and was irradiated for 10 more minutes. Finally, the box was slid to uncover another $\frac{1}{3}$ of the cell, which was irradiated for 10 more minutes. This gave six distinct regions with exposure times ranging from 0 to 50 minutes, in 10 minute steps. Making these six regions on the same cell was more difficult than making six different cells irradiated for different times. However, it ensured that the secondary variables which are uncontrolled between samples, such as polyimide layer coating, the rubbing strength and liquid crystal layer thickness, were controlled. The cell was then viewed under crossed polarizers, with the alignment of the cell at 45 degrees with respect to the polarizer and analyzer to allow maximum intensity, and heated using an Instec heating stage. The temperature was set to 68°C, and raised at a rate of 0.25°C/min. Each region of the cell was viewed and the temperature of the nematic to isotropic transition was recorded. The transition temperature was then plotted against irradiation time. The results are displayed in table 1.

Table 1: Nematic to isotropic transition temperature compared with irradiation time.

Irradiation Time (mins)	**T_{NI} (°C)**
0	68
10	69
20	69.5
30	69.5
40	69.5
50	69.5

It is clear from the table that once the cell has been irradiated for about 20 minutes, we have effectively reached full polymerization. It should be noted that if the concentration of reactive mesogen were increased, the cell would be further polymerized, and may require a different exposure time. It should also be noted that a similar test is not done with the

homeotropic cells. This is because it is assumed that the polymerization process is not dependent upon the orientation of the polymer.

3.4 Development of the Corona Source

Most of the experiments were done with the corona electron source, which was developed before the gas electron multiplier, and was used to test the liquid crystal layers from the outset of the experiment. To make our corona source, the following method was used. A piece of thin wire, with a radius of 2 mm, was sharpened to a point using a file. An image of the tip is shown in figure 10.

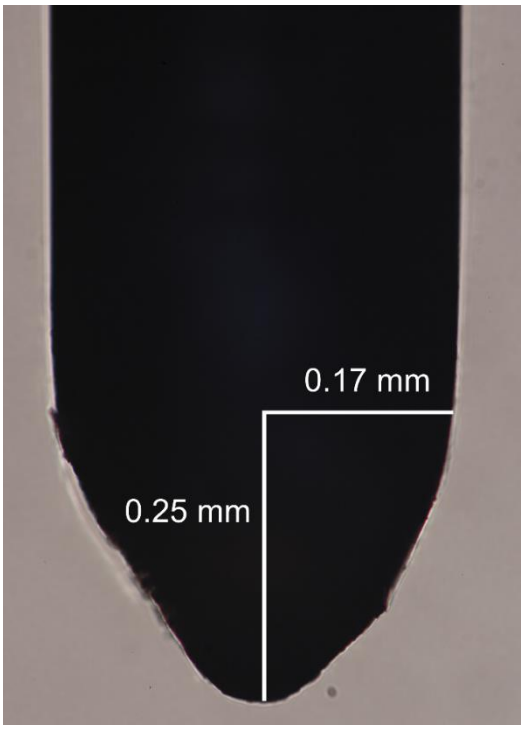

Figure 10: Image of the sharpened wire used in the corona discharge source. Dimensions of the tip are labeled.

The tip was then mounted onto a glass slide, with the tip pointing downward. Then, two grids with a sieve opening of 0.234 mm, were placed beneath this at a distance of 3 mm and 6 mm from the tip, respectively. These components were all held together by plastic walls on the sides.

The samples in all tests were placed 9 mm below the tip. An image of the corona source is shown in figure 11.

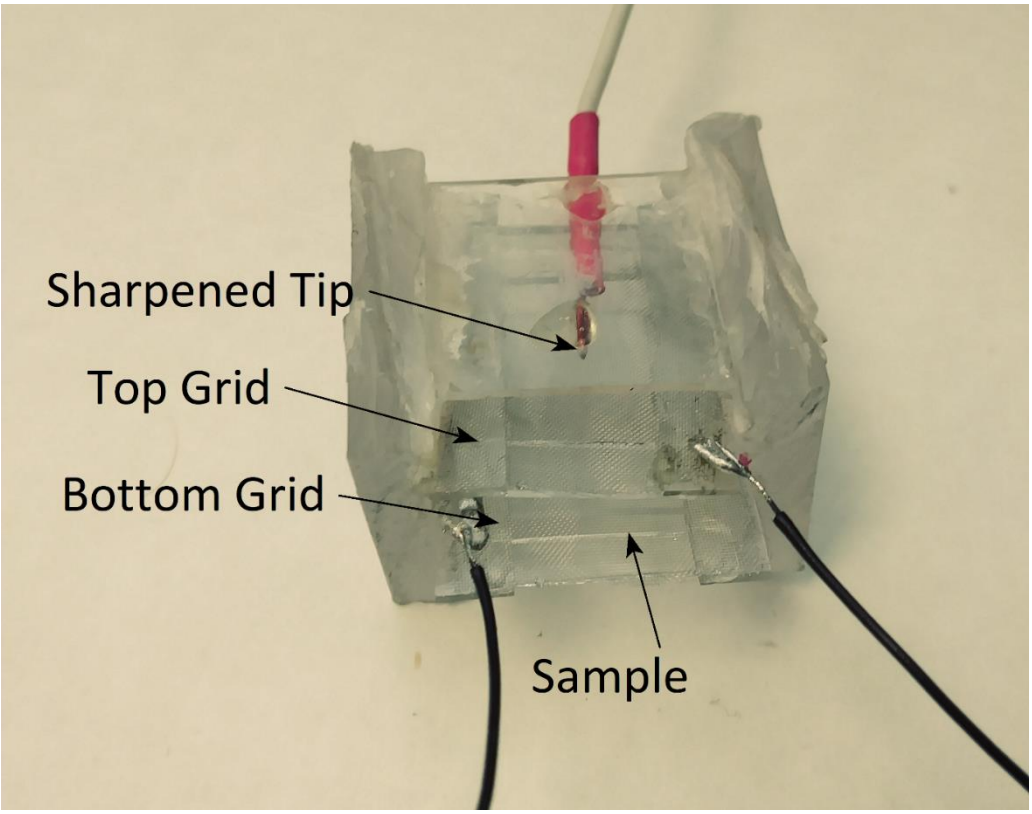

Figure 11: An image of the corona discharge source, with components labeled.

A microscope image of the mesh used in the corona source is shown in figure 12.

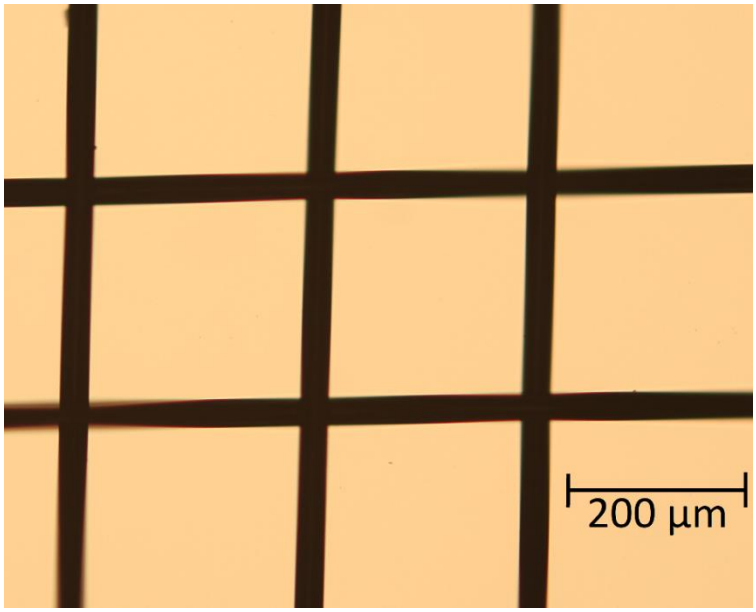

Figure 12: The fine mesh used as the grids throughout the project.

It is important to know the potential of the corona source over all space. Because of the complicated arrangement of the conductors, it is not reasonable to attempt to solve this analytically. Instead, this will be done numerically, using the relaxation method[3]. The details of the code which was written to solve for the potential are explained below.

The relaxation method is an iterative process, whereby a solution to Laplace's equation can be approximated accurately. We imagine the three dimensional volume, V, being divided up into small subdomains of area $\Delta x \Delta y \Delta z$. In each of these subdomains, the potential is approximated to be constant throughout the domain. Let us say that the potential in the volume is given by, $\Phi(x, y, z)$. Now if the subdomains are small enough, the second derivative of the potential for some subdomain located at (x, y, z) can be approximated using center differencing:

$$\frac{\partial^2 \Phi(x,y,z)}{\partial x^2} \approx \frac{\Phi(x+\Delta x, y, z) - 2\Phi(x,y,z) + \Phi(x-\Delta x, y, z)}{\Delta x^2},$$

$$\frac{\partial^2 \Phi(x,y,z)}{\partial y^2} \approx \frac{\Phi(x, y+\Delta y, z) - 2\Phi(x,y,z) + \Phi(x, y-\Delta y, z)}{\Delta y^2},$$

$$\frac{\partial^2 \Phi(x,y,z)}{\partial z^2} \approx \frac{\Phi(x,y,z+\Delta z) - 2\Phi(x,y,z) + \Phi(x,y,z-\Delta z)}{\Delta z^2}$$

Now, the solution to Laplace's equation is given by:

$$\nabla^2 \Phi(x,y,z) = 0$$

Since we have chosen arbitrary size for $\Delta x, \Delta y, \Delta z$ it must be that, to be true in general, the second derivative along each direction must be zero. This gives three equations:

$$\Phi(x+\Delta x,y,z) - 2\Phi(x,y,z) + \Phi(x-\Delta x,y,z) \approx 0$$

$$\Phi(x,y+\Delta y,z) - 2\Phi(x,y,z) + \Phi(x,y-\Delta y,z) \approx 0$$

$$\Phi(x,y,z+\Delta z) - 2\Phi(x,y,z) + \Phi(x,y,z-\Delta z) \approx 0$$

Which can be added together and rearranged to give:

$$\Phi(x,y,z) \approx \frac{1}{6}[\Phi(x+h,y,z) + \Phi(x-h,y,z) + \Phi(x,y+h,z) + \Phi(x,y-h,z) + \Phi(x,y,z+h) + \Phi(x,y,z-h)]$$

Where we have taken $\Delta x = \Delta y = \Delta z = h$. We can interpret this as saying that an estimate of the potential can be found by ensuring that each point in the 3D space is the average of the six cross points around each point (x, y, z). To do this, we will first define Dirichlet boundary conditions by specifying the voltage on each of the conductors in the region. Then, for the region of the space V which is not occupied by the set of conductors, the average of the surrounding cross of points is found, and each point in V is replaced by this average. This is then done iteratively, until convergence is reached.

This iterative method was programed into Mathematica. To simulate the experimental setup, the tip was set at -3500 V, the top grid was set at -800V, the bottom grid was set at -500V and the bottom plate was set at 0V. This produced the "heat map" of equipotential surfaces as is shown in figure 13.

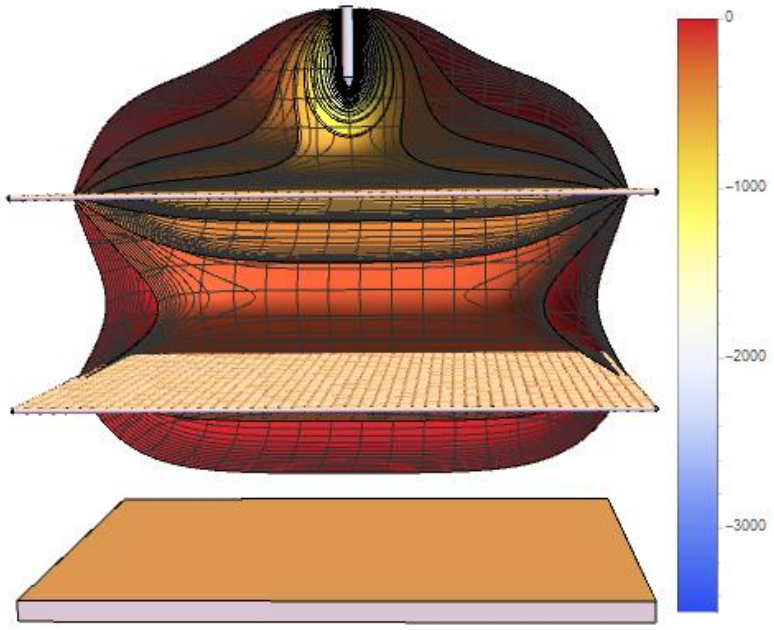

Figure 13: Figure showing the equipotential surfaces of the corona source in normal use.

Determining the properties of the voltage is important for a few reasons, each of which is key for justifying the use of the corona source in testing the liquid crystal layers. First, this map shows that the voltage across the liquid crystal layers due to the conductors is small, which is not obvious a priori. Second, it shows that, near the middle of the corona source between the bottom grid and the grounded ITO plate, the equipotential lines are nearly parallel to the liquid crystal layer. This will allow us to make several approximations about the liquid crystal layer. A 2D profile of the electric field in this region is shown in figure 14.

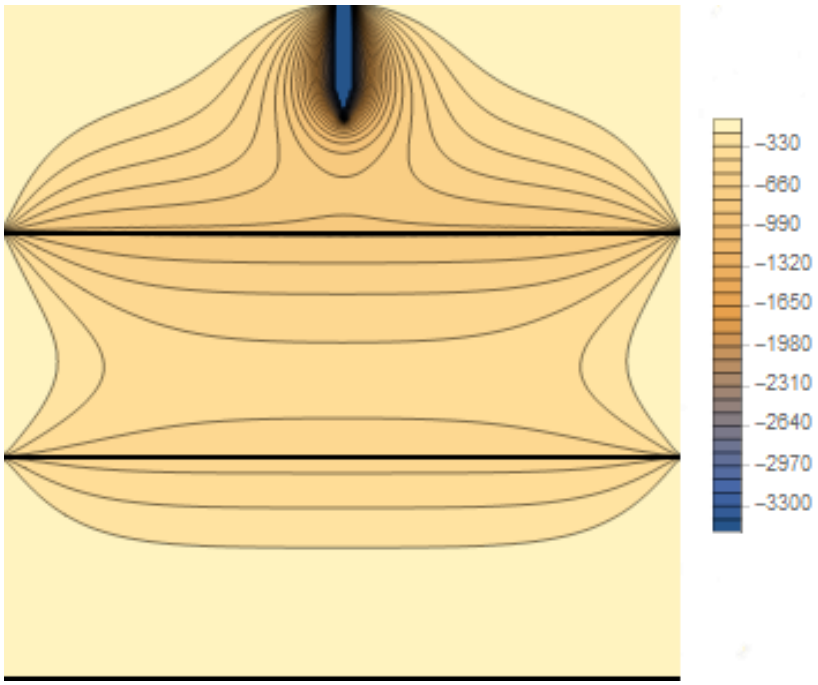

Figure 14: 2D profile of a center slice of the potential, which passes through the sharpened tip. The position of the two grids are shown by the black lines. The position of the ITO is show by a black line at the bottom of the image.

When discussing the development of the corona source, one of the primary concerns was that, when a set of conductors held at thousands of volts was placed above a grounded plate, the arrangement might lead to a potential of a few volts in magnitude across the liquid crystal layer. These few volts may be enough to cause a transition in the liquid crystal layers. This would lead to a transition in the liquid crystal layer when the corona source was on, and no transition when the corona source was off, which would be a false positive. In showing that the potential across the liquid crystal is quite small, ~90 mV when considering a 1 μm film, we can be confident in proceeding. This is, of course, considering the grids and slides are all parallel, which will be attempted to be achieved throughout the experiment.

It is also important to keep in mind that this is meant to approximate the gas electron multiplier, which will be a series of parallel grids. These parallel grids will set up equipotential

surfaces which are very nearly parallel to the liquid crystal interface. By seeing that we nearly have this at the bottom of the corona source, we can be more confident that this is a reasonable approximation of the final chamber.

As a final exercise, we will also consider the bottom grid being held at +500 V. In the project, the bottom grid will be used as a valve to control the current reaching the bottom layer. By applying a positive voltage to the bottom grid, the electrons will be unable to reach the liquid crystal layer. The potential was solved numerically, and is again graphed in figure 15 below.

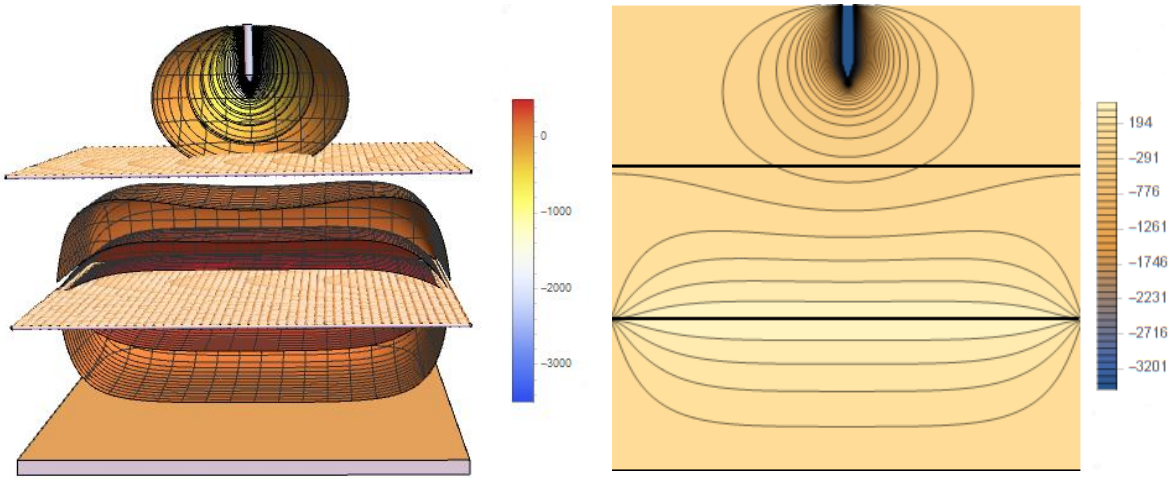

Figure 15: Heat map of potential with a positive bottom grid showing the equipotential surfaces (left) and 2D equipotential lines of the central slice of the potential (right). The position of the two grids are shown by the black lines. The position of the ITO is show by a black line at the bottom of the image.

This again shows that the equipotential surfaces are parallel to the ITO plate and contribute about ~90 mV across the liquid crystal layer, which is not nearly enough to cause a transition.

3.5 Development of Gas Electron Multiplier

During this experiment we have also created a gas electron multiplier, which is a more realistic application of the electron detector. A picture of the gas electron multiplier we developed is shown in figure 16, and a cutaway is shown in figure 17.

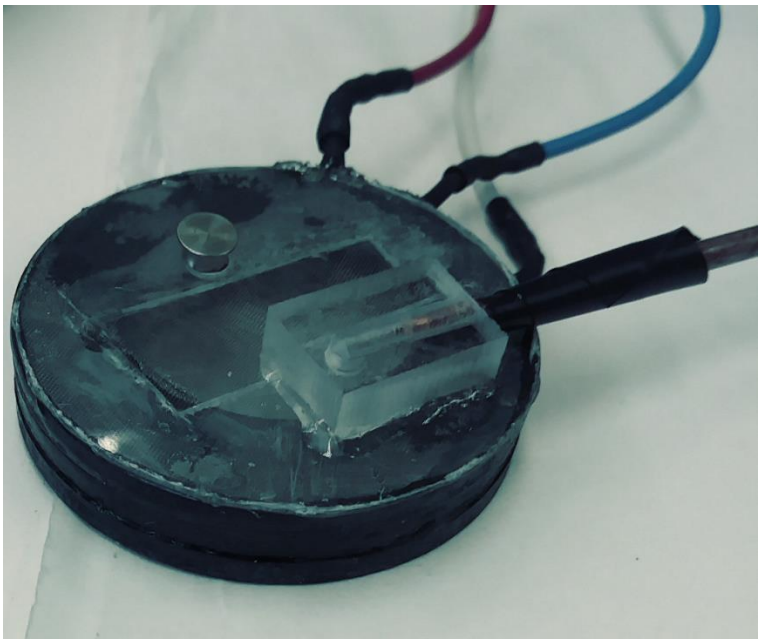

Figure 16: Image of the gas electron multiplier used in this project.

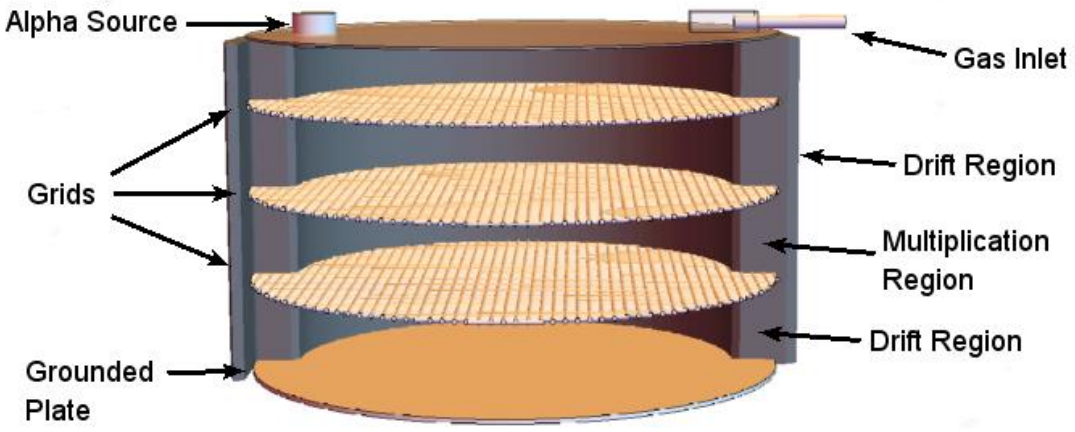

Figure 17: Cutaway of the gas electron multiplier with the regions labeled.

In this setup a small piece of americium emits alpha particles into a region of moderate electric field. The americium is set on top of one grid having a high negative voltage applied to it. Below this, there are also two more grids, with the voltage magnitude decreasing

monotonically downward toward the grounded sample. Each of the three grids have a spacing of 3.1 mm. When in operation, the potential difference between the top two grids is a few hundred volts, the voltage difference between the middle two grids is a few thousand volts, and the potential difference between the bottom grid and grounded plate is a few hundred volts. This whole arrangement is set in an enclosure, which is then flooded with a gas composed of 90% argon and 10% methane through the $1/8^{th}$ inch tubing installed through the top plate at standard pressure. When the alpha particle passes through the gas between the top two girds, it collides with the argon gas and ionizes it, producing a trail of electrons. Argon is chosen, because it not electronegative. This means that it has a negligible cross section for electron attachment. This is not the case for oxygen, water vapor or many other gasses. By minimizing electron attachment, we are guaranteed that unbound electron will reach the sample below.

The electrons produced at the top of the chamber then drift downward toward the sample, propelled by the electric field set up between the top two grids. They then enter the region of higher electric field between the two center grids. This uniformly accelerates the electrons in the trail, causing them to collide with the surrounding gas, beginning a Townsend avalanche and multiplying the number of electrons. Finally, the electrons reach the region of smaller electric field between the bottom grid and the grounded plate, which causes them to drift downward toward the sample with less energy, and effectively produces no ionization events. This will deposit a line of charge on the sample below, which will be only slightly more spread out than the line of charge at the top of the chamber, due to diffusion from collisions with the gas. This will be given a numerical value in section 3.8, when the Boltzmann transport equation for the gas electron multiplier is solved numerically.

The electrical connections of the gas electron multiplier were different from the corona discharge source. It was required that there be three separate power sources to allow for each of the grids to be held at separate potentials, much like the corona source. In addition to this, however, an amplifier was needed to be able to read the small currents received at the bottom plate. This amplifier was extremely sensitive, and amplified small ambient noise up to a few mV. To counteract this, all exposed electrical components needed to be grounded in a star pattern to prevent ground loops. Also, the chamber and wiring needed to be wrapped in a makeshift Faraday cage to minimize noise pickup.

3.6 Numerical Analysis of Electron Motion

As the electrons move through air, they are accelerated by the electric field, but also constantly lose energy through collisions with air molecules. This balance between gaining energy from the electric field and losing it through collisions will establish the energy of the electrons. It is important to develop some estimate for the energy of the electrons as it will be important in determining how the electrons reaching the liquid crystal layer will behave. It is also of interest to understand the distribution of electrons reaching the liquid crystal layer. Generally, the average energy and distribution of the electron swarm can be found by solving the Boltzmann transport equation. This is usually very difficult, and often done numerically. The basic idea, however is outlined here.

At the energy of a few eV, electrons will interact with the surrounding gas molecules in the following ways: momentum transfer, low-energy excitations and attachment[4]. In some cases, the electron will scatter elastically off of the gas molecules. In some cases, the electron will scatter inelastically, transferring some of its energy to the internal degrees of freedom within the

atom. It may also attach itself momentarily to the atom, in a process called electron attachment, which is represented as:

$$e^- + X \Rightarrow X^- \Rightarrow e^- + X$$

The Boltzmann transport equation describes the evolution of a function, f which consists of seven variables: three position coordinates, three velocity coordinates and one time coordinate. The most general equation is written as[5]:

$$\frac{\partial f}{\partial t} = \left(\frac{\partial f}{\partial t}\right)_{force} + \left(\frac{\partial f}{\partial t}\right)_{motion} + \left(\frac{\partial f}{\partial t}\right)_{collision}$$

This is the statement that the time evolution of the system can be decomposed into a linear combination of each of the ways that the state may change; through an applied force, through the free motion of the particles, and through collisions of the particles with each other and their surroundings. Now we are able to apply this to our system in particular.

The force term is found easily enough. The only force acting on the electrons and ions is the electric field. This is given by $\vec{F} = e\vec{E}$, meaning that the force term is given by $\left(\frac{\partial f}{\partial t}\right)_{force} = \frac{e}{m}\vec{E} \cdot \vec{\nabla}_v f$. We can also make the assumption that the particles move ballistically between each of these collisions. This can be written as $\left(\frac{\partial f}{\partial t}\right)_{motion} = -\vec{v} \cdot \vec{\nabla} f$. The collision term is much more complicated, since it will involve the differential cross sections for each possible interaction between the electron and each species of gas, which will in turn depend on f. We can just consider it a function of f like so: $\left(\frac{\partial f}{\partial t}\right)_{collision} = C[f]$. Putting these equations together, we get:

$$\frac{\partial f}{\partial t} + \vec{v} \cdot \vec{\nabla} f - \frac{e}{m}\vec{E} \cdot \vec{\nabla}_v f = C[f]$$

This can then be solved numerically by integration, given the cross sections. The cross section values have been taken from the Plasma Data Exchange Project LxCat[6]. These cross sections are calculated using scattering theory, and not measured values.

There are many programs designed to solve the Boltzmann transport equation. The program METHES is used here, which is a Boltzmann transport equation solver in Matlab, which has been modified for this project[7]. The program works by further simplifying the collision term of the Boltzmann transport equation. The pressure of the gas sets a characteristic length scale over which the electrons move ballistically, without collision. When a collision does occur, it affects the velocity of the particles but does not change the position of the particles. The particles then travel ballistically again, gaining momentum from the electric field. This program uses the cross section of each of the gas species and a random number generator to choose which collision occurs at each step of the process. This program can be used to simulate the trajectory of the individual particles, the motion of a swarm of electrons for some time, or to find solutions when the system has reached energetic equilibrium. While this program takes longer to run than some others, it does offer much more data, and a much clearer picture of how the electron distribution changes in time.

3.7 Electron Motion in the Corona Source

First, we will outline what approximations will be made and numerical values which are used when analyzing the corona source. The air filling the corona source will be modeled to contain 78% Nitrogen, 20% Oxygen and 2% H_2O, to reflect air with moderate humidity[8]. This information will further weigh the likelihood of collisions between the electrons and the individual gas species. The pressure will be 100 kPa (1 atm). Finally, we must determine the electric field. The electric field of the corona source is rather complicated, as we have seen

before, and not easily solved analytically. However, the field it not terribly difficult to find if each of the three regions are considered independently, and the effect each region has on its neighboring regions is ignored. The region between the two grids, and between the bottom grid and the grounded plate, will be taken to be constant in the z direction. This is effectively using the parallel plate approximation for the grids. To proceed, we will consider the electrons being generated at the sharpened tip, and being accelerated through each of the regions. We will follow their spatial distribution throughout their motion, and will record their final distribution and the distribution of their energy when reaching the liquid crystal layer.

To be able to solve in each of the regions, we will need to find expressions for the electric field. In normal operation, the corona source will have ~ -3500 V on the tip, -800 V on the top grid and -500 V on the bottom grid. The electric field in all of these regions can be calculated as follows. Let us consider the region between the tip and the top grid. This region would be difficult to solve analytically, but can be done using approximations like a truncated tip, or an expansion of the asymptotic forms of the potential. Instead of these methods, this region will be treated numerically, based on the work which has already been done. We can already solve the potential in this region using the relaxation method, and can use finite differencing to find the electric field. This was done by discretizing space into cubes having a side length of 38μm. In these cubes, the potential is constant. Then, the electric field in each of these regions was found using center differencing. So, the volume in this region is being modeled as a set of cubes of side length of 38μm, each having a constant electric field. As the electrons move, they enter these regions, and experience an abrupt change in the electric field.

For the regions of the corona source between the top and bottom grid and the bottom grid and the grounded plate, a parallel plate approximation will be used to find the electric field.

Using that the potential on the top grid is – 800V and the potential on the bottom grid is -500V and that they are each spaced apart by 3 mm, we can write the total electric field as being:

$$\vec{E}(\vec{x}) = \begin{cases} \vec{\nabla} V_{relaxation}(x) for\ 9\ mm \geq z > 6\ mm \\ -1 * 10^5\ for\ 6\ mm \geq z > 3\ mm \\ -1.6 * 10^5\ for\ 3\ mm \geq z > 0\ mm \end{cases}$$

First, let us find the distribution of electrons on the surface of the liquid crystal. In the regions between the two grids, and between the bottom grid and the grounded plate the electric field is constant, and therefore independent of position. Since the collision term in this formulation of the Boltzmann transport equation is also independent of position, equilibrium between the energy gained from the electric field and lost due to collisions will be reached. Once it is reached, the evolution of the distribution of particles is well defined and can be extrapolated. This was used to reduce computation time. When particles reach equilibrium in a constant electric field, they continue to spread out in a Gaussian fashion due to the collisions. This means that we will get some distribution of electrons exiting the top region of the corona source, which will be spread out in some well-defined way in the bottom two regions. It was found that the spreading of the electrons in the plane parallel to the ITO surface in the region between the two grid is $\sigma^2 = \ 2.0 * 10^{-5} m^2$. It was found that the spreading of the electrons in the region between the bottom grid and the ITO was $\sigma^2 = 2.7 * 10^{-5}\ m^2$. So, the total spreading of the electrons along the plane parallel to the ITO surface through the bottom two regions is $\sigma^2 = 4.7 * 10^{-5}\ m^2$.

For the top region, no approximation can be made. The electric field is too complicated to allow for steady state to be reached. Instead, the program was allowed to run in its entirety. The electron swarm was initialized at the tip of the corona source. The electrons were then allowed to drift downward, until reaching the top grid. The distribution of the electron swarm was recorded

at the top grid, and then diffused according to the standard deviations found above. This final distribution was then taken to be the distribution of electrons on the liquid crystal layer. In figure 18, we have plotted the distribution of electrons on the liquid crystal layer and have also fitted a proposed functional form.

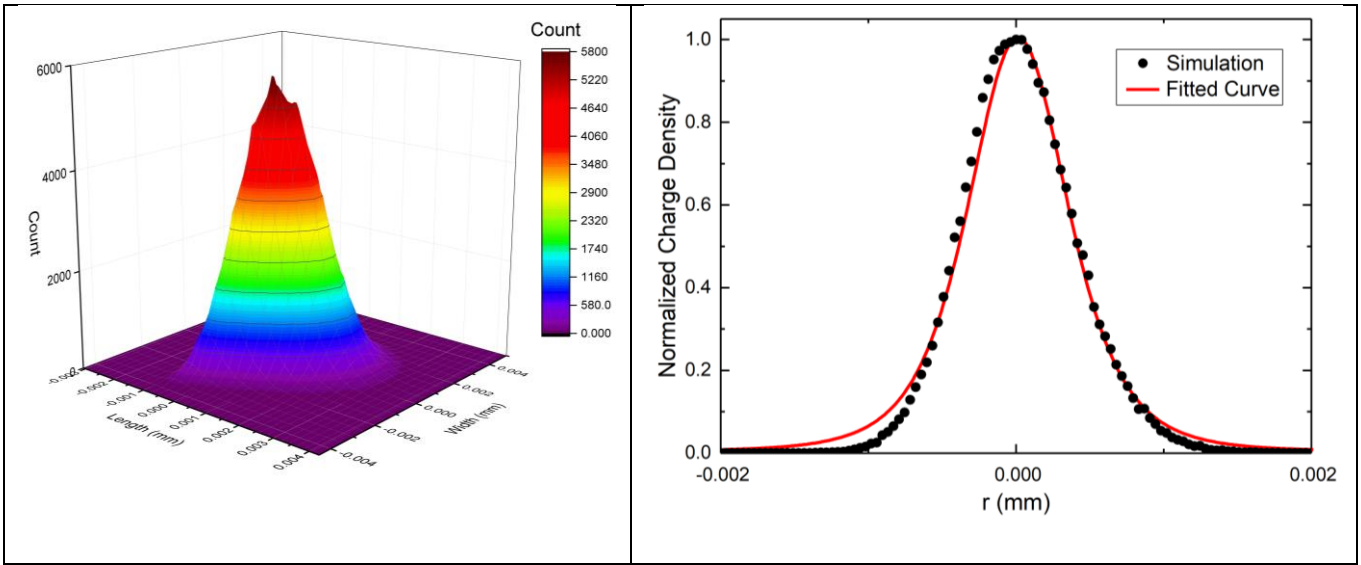

Figure 18: 3D distribution of particles on the liquid crystal upon exiting the corona discharge source (left). The center cross section of the distribution was taken, and fitted with a proposed functional form. The proposed functional form $Q(r,\theta) = A\cos^5\left(\arctan\left(\frac{r}{R}\right)\right)$.

The proposed functional form of the charge density on the liquid crystal layer is $Q(r,\theta) = A\cos^5\left(\arctan\left(\frac{r}{R}\right)\right)$. The constant R was found to be of best fit when R = 1 mm. This form is encouraging, since it agrees with previously known forms of the charge density for a corona source in the simple geometry of a single tip and grounded plate[9]. Although our corona source is not the same physically, the setup is similar, so the functional form should be as well.

It was found that energetic equilibrium is reached in the region between the bottom grid and the liquid crystal. This means that the distribution in energy of the electrons reaching the liquid crystal is the equilibrium distribution. This energy distribution for electrons exiting the corona source is shown in figure 19.

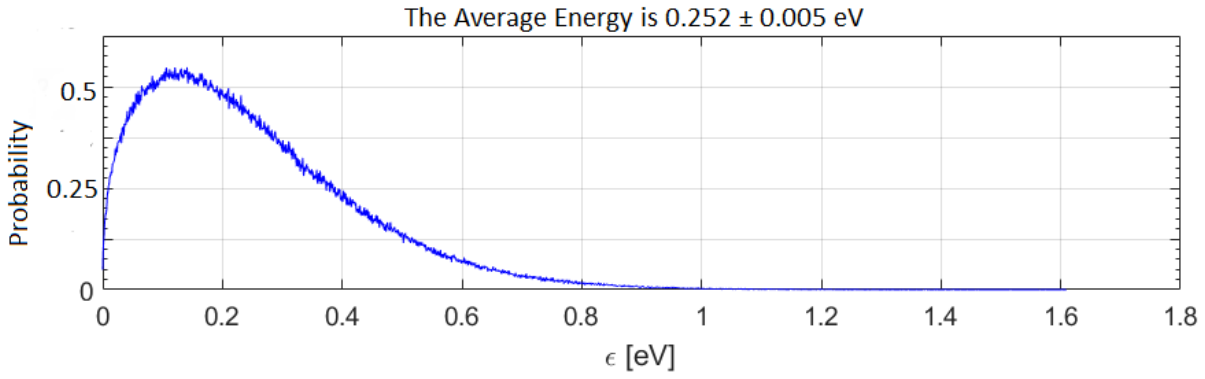

Figure 19: Energy distribution of particles exiting the corona discharge source.

3.8 Electron motion in Gas Electron Multiplier

To analyze the gas electron multiplier, similar approximations as the previous section will be made. The region will be modeled to contain 90% Argon and 10% Methane, and will be at a pressure of 100 kPa (1 atm). The gas electron multiplier will be approximated as three regions, each bounded by parallel plates with a constant voltage applied. This will be a reasonably good approximation for finely spaced mesh. This approximation gives rise to a simple electric field, which is constant in the z direction. In the expected mode of operation, the top grid will be held at – 2200V, the center grid will be held at -2000V and the bottom grid will be held at -200V. Using that each grid is spaced at a distance of 3.1mm apart, we can compute the electric field as being

$$\vec{E}(z) = \begin{cases} -6.4 * 10^4 \frac{V}{m}\, \hat{z}\ for\ 9.3\ mm \geq z > 6.2\ mm \\ -6.4 * 10^5 \frac{V}{m}\, \hat{z}\ for\ 6.2mm \geq z > 3.1\ mm \\ -6.4 * 10^4 \frac{V}{m}\, \hat{z}\ for\ 3.1\ mm \geq z > 0\ mm \end{cases}$$

Now, we are also able to choose an initial configuration for the charges. We will say that when the alpha particle is emitted into the chamber, it leaves behind a track which has a width of ~100 μm and with a length of ~ 10 mm. This initial distribution is shown in figure 18.

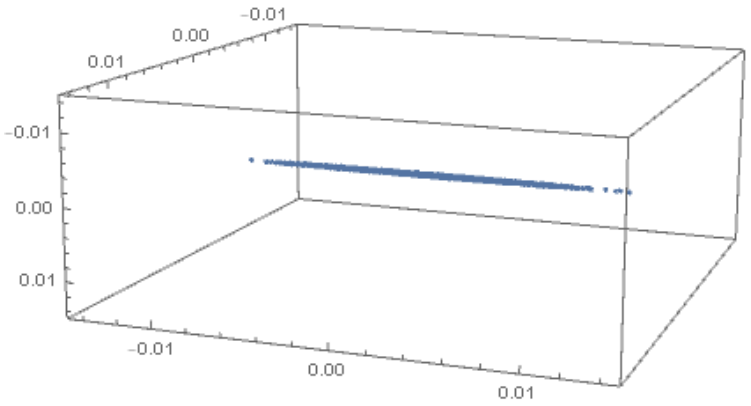

Figure 20: The initial distribution of the electrons entering the gas electron multiplier.

If we would run the program and choose it to terminate when the electron swarm reaches the bottom of the chamber, it would take a very long time to compute. We are able to use a similar line of reasoning as was done for the corona source, to find the equilibrium spreading, and to extrapolate the spreading of the electron swarm. In this case, we are able to do this for all three regions. It was found that in the region between the top grid and the center grid, the increase in the variance of the electrons in the direction parallel to the grids is $\sigma^2 = 2.0 * 10^{-6} m^2$. This was the same variance when the particles travel between the bottom grid and the ITO, since the electric field is the same. The increase in the variance of the electrons in the direction parallel to the grids when traveling between the center and bottom grid is $\sigma^2 = 4.2 * 10^{-4} m^2$. This means that the total increase in variance along the direction parallel to the grids when traveling through the entire system is $\approx 4.2 * 10^{-4} m^2$.

Using this information, the distribution of the particles can be found and plotted. This is shown in figure 21.

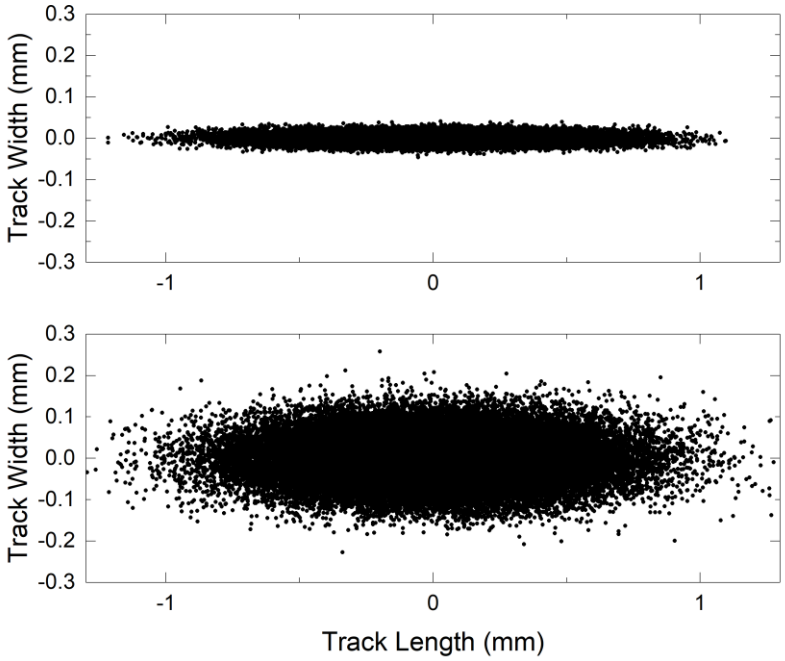

Figure 21: Distribution of electrons in the xy plane entering the gas electron multiplier (top), and the distribution of electrons deposited on the liquid crystal surface after exiting the gas electron multiplier (bottom).

This shows that the spreading along the direction of the alpha particle is negligible but the spreading of the track transverse to the direction that the alpha particle travels is not.

It was found that energetic equilibrium is reached in the region above the liquid crystal. This means that the distribution in energy of the electrons reaching the liquid crystal is the equilibrium distribution. This energy distribution is shown in figure 22.

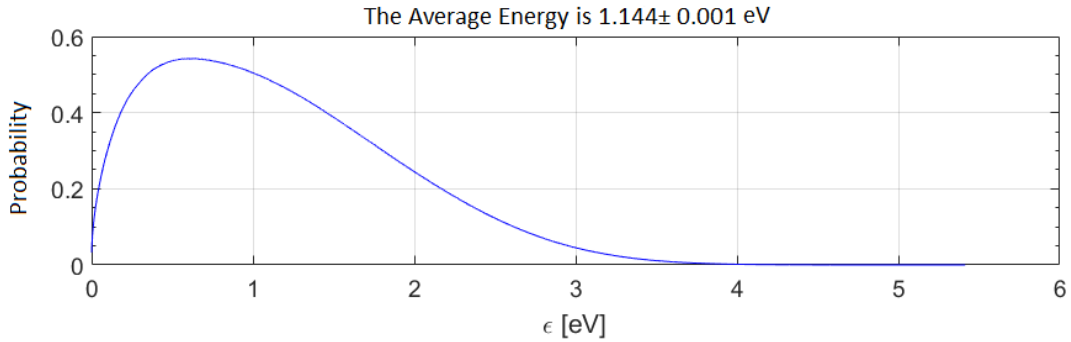

Figure 22: Energy distribution of the particles exiting the gas electron multiplier

Chapter 4

Experimental Work with Liquid Crystal

Prior to beginning testing with the electron sources, some basic understanding of the liquid crystal layers was needed. The corona source and the liquid crystal layers were developed in parallel, meaning that some references to the corona source will be made here, but the devices used and tests associated with them specifically will be better described later.

4.1 Hybrid Layer Thickness Optimization

When creating samples of liquid crystal by spin coating, it was important to optimize the thickness of the liquid crystal. The variable which most influences the thickness of the layers was found to be the concentration of the liquid crystal and reactive mesogen in the solvent. The thickness of the layer was much less significantly affected by the amount of this solution which was placed on the slide and the spinning speed, so both of these variables were held constant throughout the test. The spin speed was kept at 1700 rpm and 25 µL of the solution was placed on a 2 cm x 2 cm slide.

Samples were prepared with 200 mg/mL, 250 mg/mL, 300 mg/mL, 375 mg/mL and 500 mg/mL solutions, giving a wide range of sample thicknesses. These were then placed under the corona source, with the top grid held at -800V and the bottom grid held at -500V. The tip of the corona source was set to deliver -2200V, but was initially in the off state. Each sample was placed under the corona source in turn, which is viewed under a polarizing microscope. The tip voltage was then quickly turned on and off again, which deposited electrons on the liquid crystal layers. The deposited electrons set up an electric field across the liquid crystal, changing the orientation of the molecules, and therefore the birefringence. When viewed through the crossed

polarizers of the polarizing microscope, an optical change is seen in the layers. In this case, a region of the hybrid layer transitions to homeotropic alignment, which causes the liquid crystal layer in this region to no longer be birefringent. This is observed as a dark patch through the microscope, since no light is able to pass through the crossed polarizers. Videos of the layers were recorded through the microscope with a CCD camera at 30 frames per second. These videos were then inspected for an observable variation dependent upon the thickness of the layers. It was noted that one of the key variables was the intensity difference between the "on" and "off" state of the liquid crystal layers.

Finding that the thickness of the layers can be optimized using the intensity is somewhat expected. It is necessary for the layers to have a certain thickness if the light is to have a significant change in its polarization, so as to allow a large fraction of light through the polarizer. If the layers were too thin, the difference between the "on" state and the "off" state would be smaller than it would be for thicker layers, because the "off" state is not as bright as it is in thicker layers. If the layers were very thick, the electrons did not seem to induce a transition uniformly throughout the layer. This is possibly due to the polymer resisting the reorientation, leading to an "on" state, which is not as dark as in thinner samples containing fewer polymer fibrils. This led to a simple criterion for optimizing the planar layer thickness: find the thickness where the normalized intensity difference between the "on" and "off" state is the largest. This will lead to an electron detector with greater contrast between the on and off state, and therefore make deposited electrons easier to detect.

The videos of each of these samples at varying concentrations was edited to contain only the region which underwent the transition from on to off. These were then analyzed frame by

frame to find the average intensity of the region in both the on state and in the off state. These average intensities are displayed in table 2.

Table 2: Intensity of the liquid crystal layers as a function of the concentration of the solution.

Molarity of Liquid Crystal Solution	Normalized Intensity Difference
200 mg/mL	0.982
250 mg/mL	0.985
300 mg/mL	0.985
370 mg/mL	0.593
500 mg/mL	0.009

This table suggests that the optimum thickness of film is obtained when the liquid crystal is diluted to 250 mg/mL or 300 mg/mL. Since the transition of thicker layers requires a lower applied current, thicker layers are better for testing under the corona source, so we will choose layers made with 300 mg/mL solution as being optimal.

4.2 Determining Hybrid Layer Thickness

In most liquid crystal cells, the Freedericksz transition voltage does not depend upon the thickness of the layers, so the thickness is not critical to measure. Operating as an electron detector, however, makes the thickness of the samples much more important to control. Since the voltage is created across the liquid crystal layer by holding charges away from a grounded plate, thicker layers will require fewer surface electrons (and therefore a lower electric field) for a transition to take place because of the reduction in the elastic energy cost. An accurate measurement of the thickness of the layers will be needed to be able to quantify what charge must be deposited on the surface to induce a transition.

To determine the thickness of the hybrid liquid crystal samples, an optical method was employed. This was done via a retardance measurement, from which the thickness of the layer was inferred. The retardation is defined to be the integrated effect that a birefringent material has

on the light passing through it. The following will briefly describe the method which will be employed. Consider a uniform layer of liquid crystal of thickness h, with its director aligned as shown in figure 23.

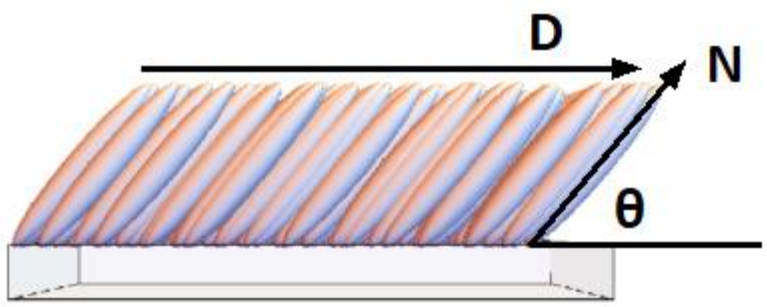

Figure 23: A layer of liquid crystal aligned along the rubbing direction D. The director, N, is tilted off of the horizontal by and angle θ.

It is known[1] that if the rubbing direction of the liquid crystal is at an angle of 45° with respect to the polarizer and the analyzer, the phase shift between the ordinary and extraordinary rays exiting the liquid crystal will be

$$\delta = \frac{2\pi D \Delta n}{\lambda} Sin^2(\theta)$$

In this experiment, we have taken measurements of the intensity of the light exiting the liquid crystal, both when the analyzer is parallel to the polarizer and when it is perpendicular to the polarizer. These intensity values are labeled as $I_{||}$ and $I_{\perp}$, respectively. The liquid crystal will absorb some of the incoming light. It can be shown[1] that the intensity is given as

$$I_{||} = I_0 Cos^2(\frac{\delta}{2}) \text{ and } I_{\perp} = I_0 Sin^2(\frac{\delta}{2})$$

Which then can be combined to yield

$$\delta = \pi K + 2Tan^{-1}\left(\sqrt{\frac{I_{\perp}}{I_{||}}}\right)$$

Where K is an integer.

We will consider a simple model for the orientation of the director throughout the hybrid layer, as shown in figure 24.

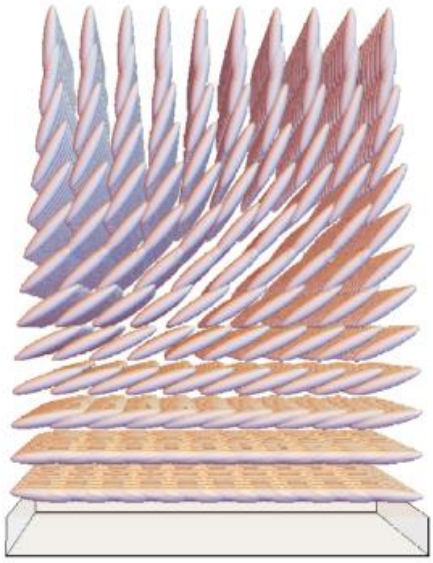

Figure 24: Alignment of an idealized hybrid cell with a twist of the director

where the relation between $\theta$and z is given by $\theta = \frac{\pi}{2\,d} z$, where z is the depth in the liquid crystal and with z=0 defined at the glass. Now, if we consider the director varying continuously throughout the cell, we can divide the liquid crystal layer into thin layers of thickness ∂h, which each contribute to the phase shift. This will lead to an approximate phase shift of

$$\partial\delta = \frac{2\pi\,\Delta n}{\lambda} Sin^2(\theta)\,\partial h$$

Then, the phase shift as a function of depth is given by

$$\partial\delta = \frac{2\pi\,\Delta n}{\lambda} Sin^2\left(\frac{\pi}{2\,d} z\right)\partial z$$

Which can readily be integrated over all z, from 0 to d to give

$$\delta = \frac{\pi \Delta n}{\lambda} d$$

Equating this with the above expression and solving for d gives the final expression,

$$d = \frac{2\lambda}{\Delta n \, \pi} Tan^{-1}\left(\sqrt{\frac{I_{\perp}}{I_{||}}}\right) + \frac{\lambda K}{\pi \Delta n}$$

Now, as the thickness of the liquid crystal increases, a larger value of K is required. To be able to determine the thickness of the liquid crystal exactly, we will need to know more information to determine K. When creating the layers, we increased the thickness by increasing the molarity of the solution used to spin coat the slides. During this process, it was not observed that the layers were thick enough to become colored. This means that the liquid crystal layer was sufficiently thin, so that the layer must be approximately the wavelength of light. This means that K = 0. Now the birefringence, Δn, of E7 is well known. $\Delta n = 0.218$ for $\lambda = 644\ nm$ at room temperature[2]. All that is left to be determined is $I_{||}$ and $I_{\perp}$. To do this, the sample was placed in a setup as shown in figure 25.

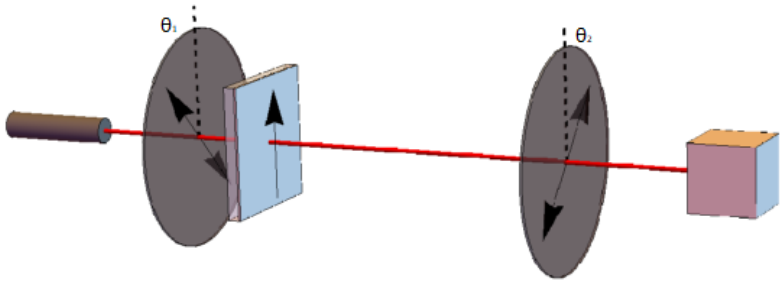

Figure 25: Experimental setup used in determining the thickness of hybrid cells.

In this setup, laser light is passed through a polarizer, through the sample, through the analyzer, and finally to the detector. The arrow on the liquid crystal sample indicates the rubbing direction.

θ_1 is kept at 45° throughout the measurement with respect to the rubbing direction of the liquid crystal layer. θ_2 is held at ±45° to measure $I_{||}$ and $I_{\perp}$ respectively. The results of this test are shown in table 3.

Table 3: Results of retardance measurements with calculated thickness.

	$\frac{I_{||}}{I_{\perp}}$	**Calculated Thickness**
Sample 1	0.747	1.31 μm
Sample 2	0.532	1.16 μm
Sample 3	0.586	1.21 μm
Sample 4	0.819	1.36 μm
Sample 5	0.719	1.29 μm
Sample 6	0.702	1.29 μm
Averaged	0.7 ± 0.1	1.27 ± 0.07 μm

Putting this together, we find that $d = \frac{2\,(632.6nm)}{(0.218)\,\pi}\, Tan^{-1}\left(\sqrt{\frac{I_{\perp}}{I_{||}}}\right) = 1.27\,\mu m$

4.3 Determining Homeotropic Layer Thickness

Determining the thickness of the homeotropic samples could not be done using the same method. The homeotropic layers do not have birefringence, so the method described in the previous section clearly will not work. We were, however, fortunate enough to have a much simpler method. To measure the thickness of the homeotropic samples, a corner of the samples was scraped off using a razor blade. The region was then cleaned by wiping with acetone and then methanol, which removed all of the liquid crystal. This was then placed under the microscope. A monochromatic filter of wavelength 545 nm was used to view the films. This allowed us to see the interference bands. If we take the index of refraction of air to be n = 1, the index of refraction of the liquid crystal[3] to be n ≈ 1.48 and the index of refraction of the glass

slide to be n = 1.53, then the bright bands occur at a thickness of $d = \frac{m\lambda}{2\,(1.48)}$, where m is an integer. By counting the number of interference bands, the value of m can be found. For thin layers, this is not a very accurate measurement, since knowing the film thickness to within $\frac{\lambda}{2\,n} \approx 185\ nm$ is not usually sufficient. It was found, however that the layers are fairly thick, so this method is able to find the thickness of the layers reasonable well. Images of the interference fringes are shown in figure 26.

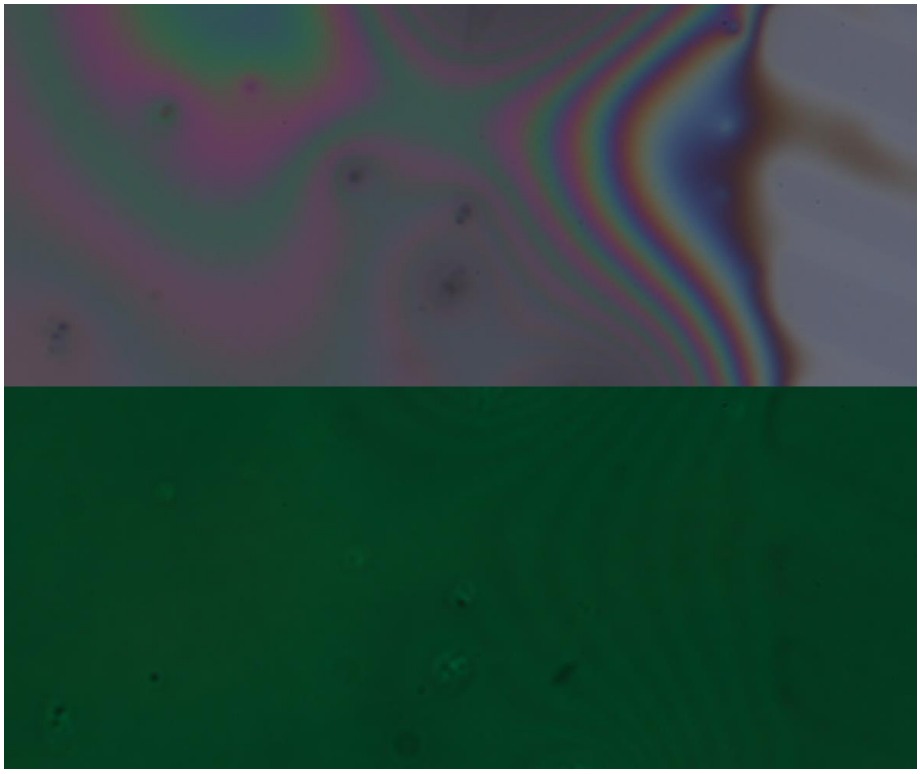

Figure 26: Images showing a region of the film illuminated using white light, taken in reflection mode without polarizers (above) and the film imaged under monochromatic light, taken in transmission mode without polarizers (below). The image above was taken with a 0.05 second exposure, while the image below required a 2 second exposure.

This was done with several regions of the cell to ensure that the thickness can be reliably measured in this way. A large portion of the cell was then observed to ensure that the liquid crystal was of uniform thickness.

The cell was observed to have approximately 7 bright interference fringes. This gives a thickness of $d = \frac{7(0.545\ \mu m)}{2\ (1.48)} = 1.29\ \mu m$.

4.4 Liquid Crystal Response Time

The response time is an important property in many liquid crystal devices. The experiment used to measure the response time of the liquid crystal to the applied electrons is similar to the experiment done in section 4.1. Both hybrid and homeotropic samples were placed under the corona discharge source. The tip was held at -2200V, the top grid was held at - 800V and the bottom grid was held at + 500V. This effectively blocked the electrons from reaching the sample below. A square pulse of width 0.5 s was applied to the bottom grid, which changed its applied voltage from + 500V to - 500V and back to +500V. This allowed electrons to pass through the bottom grid and reach the sample below for 0.5 s. The intensity of the liquid crystal layers was recorded through the microscope using a photodiode. By plotting the intensity data as a function of time, the response time of the liquid crystal can easily be determined. A graph of the hybrid an homeotropic switching is shown in figure 27.

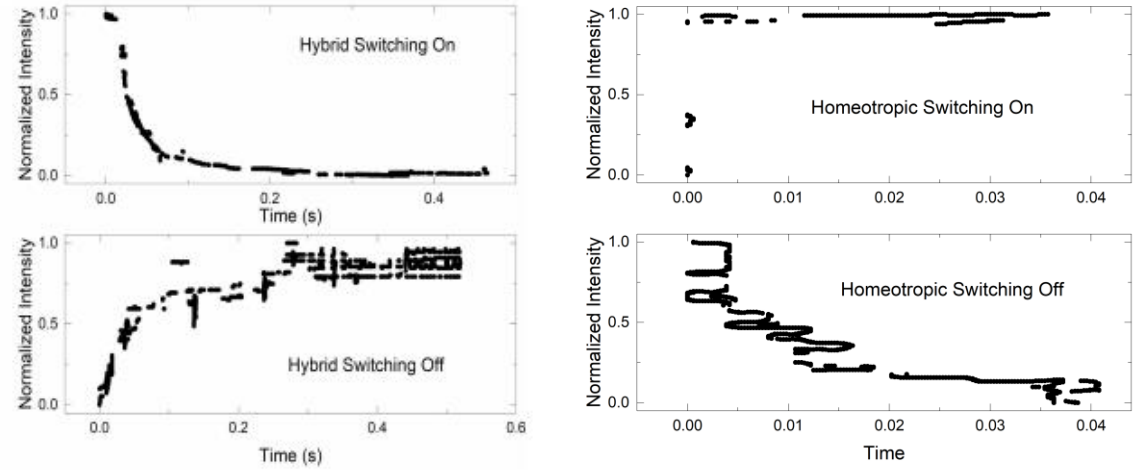

Figure 27: Data from hybrid aligned layer, shown in black circles.

The experimental data was fit with the appropriate exponentials, and the liquid crystal response time taken to be is the time constant of these exponentials. These time constants are recorded in table 4.

Table 4: Time Constants for Hybrid and Homeotropic Layers

	On	**Off**
Hybrid	25 ms	77 ms
Homeotropic	2 ms	15 ms

It must be noted that in this test, the time constant of the homeotropic layers is more accurate than the time constant of the hybrid layers, and both depend on the layer thickness This is because of the Freedericksz threshold voltage of the homeotropic layers, which is absent from the hybrid layers. The homeotropic layers will transition sharply when enough charge has been deposed on the liquid crystal layer, and switch off again when enough of the charge has migrated to ground. The hybrid layers, on the other hand, will begin to transition to homeotropic alignment as soon as charge is deposited on the layer, and will begin to revert back to hybrid alignment as charges begin to migrate to ground. Because of this, the time constant for the hybrid layer turning on is not a good measure of the time constant of the liquid crystal, because it can be imagined that if charge were deposited more slowly on the layer, which can be done by applying a smaller current, the effective time constant would be larger. The hybrid time constant for transition to the off state also includes the time that the charges take migrate to ground. If it is assumed that the charges migrate to ground at the same rate for all layers, this measurement is a reliable one. The homeotropic sample does not have this problem, and so is a good measure of the time constant.

Chapter 5

Experimental Work with the Corona Source

From the beginning of the project, the corona source was used to test the liquid crystal layers. This setup had many limitations, but I was able to make some key measurements, which ultimately culminated in an estimate for the charge density accumulating on the surface of the liquid crystal. This measurement was used to estimate the voltage across the layer, which was then shown to be in good agreement with the known transition voltage thresholds of the liquid crystal.

5.1 Demonstrating the Corona Source

As an initial test, it was shown that the corona source could be used induce a transition in the liquid crystal layers. Initially, this was done with a simple sharpened wire and a loop as shown in figure 28.

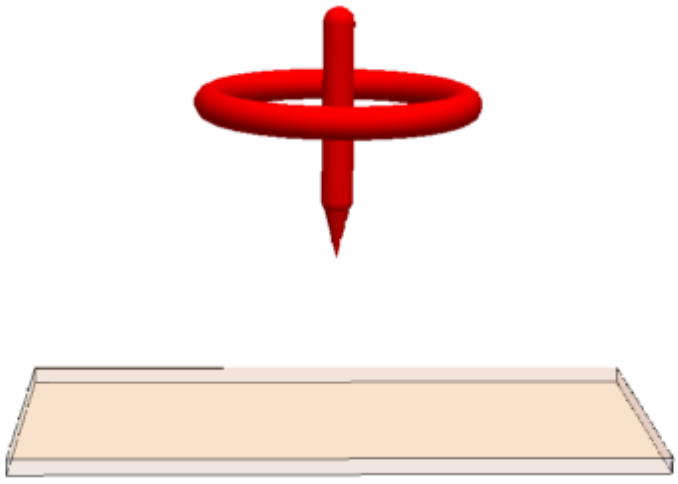

Figure 28: Single loop of wire with a sharpened point above a grounded plate coated with liquid crystal.

This is the most basic design for a corona discharge source. The sharpened tip allows for the Townsend avalanche, while the loop of wire dispelled the ions in the air, to keep the current flowing freely. Both the tip and the loop were held at the same voltage. This setup did not allow for fine control over the current reaching the layers, did not have nice equipotential lines and was not as stable as later designs. It was, however, quick to build and allowed for initial tests to show proof of concept. Samples were placed below this source, and the tip was turned off and on. The results of these initial tests are shown in figure 29.

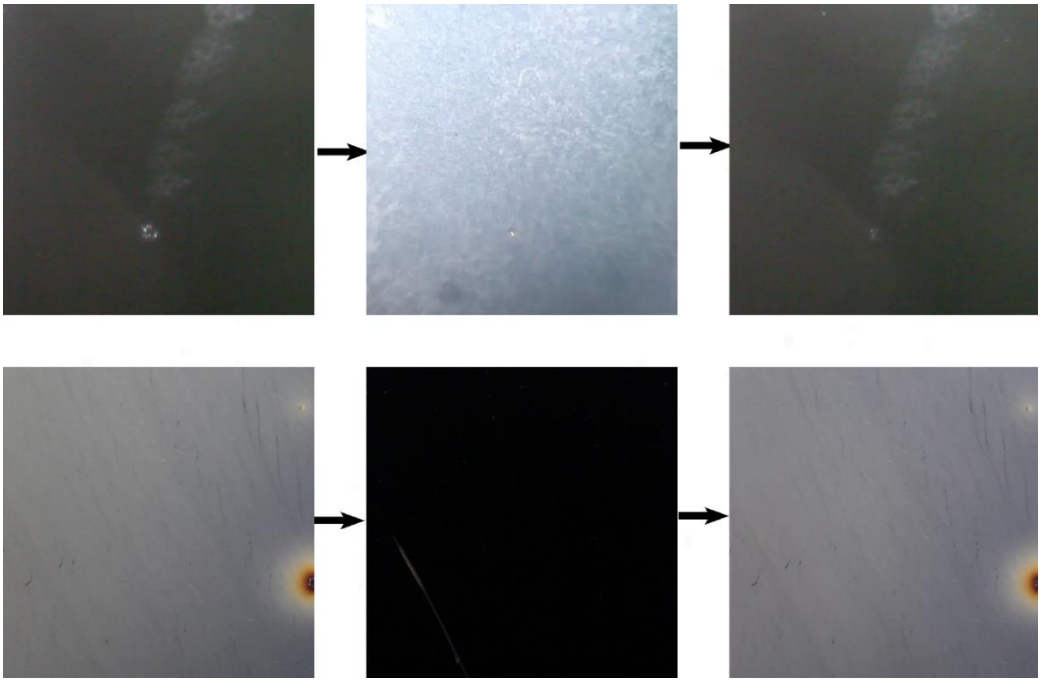

Figure 29: Initial tests of the corona discharge source for the homeotropic (top) and hybrid (bottom) cells. The first column of images shows the samples prior to use. The center column shows the samples with the tip and ring having a large negative voltage applied. The last column shows the samples after the tip and loop have been turned off again.

As another initial test, to see whether the direction of the corona source could be accurately controlled, a device was made as shown in figure 30. Two thin coaxial metal rings were affixed with three sharp metal points spaced at 120° from each other. The outer ring acted as support, while the inner ring dispelled ions around the sharpened tips. This entire system was

then held at a high negative voltage above the liquid crystal layer, which was grounded. This acted as a corona source with three distinct source points. Images of the surface were taken through the central hole.

Figure 30: The arrangement of the metal ring and spikes for tests involving several corona showers.

Images of these three distinct circles are shown in figure 31.

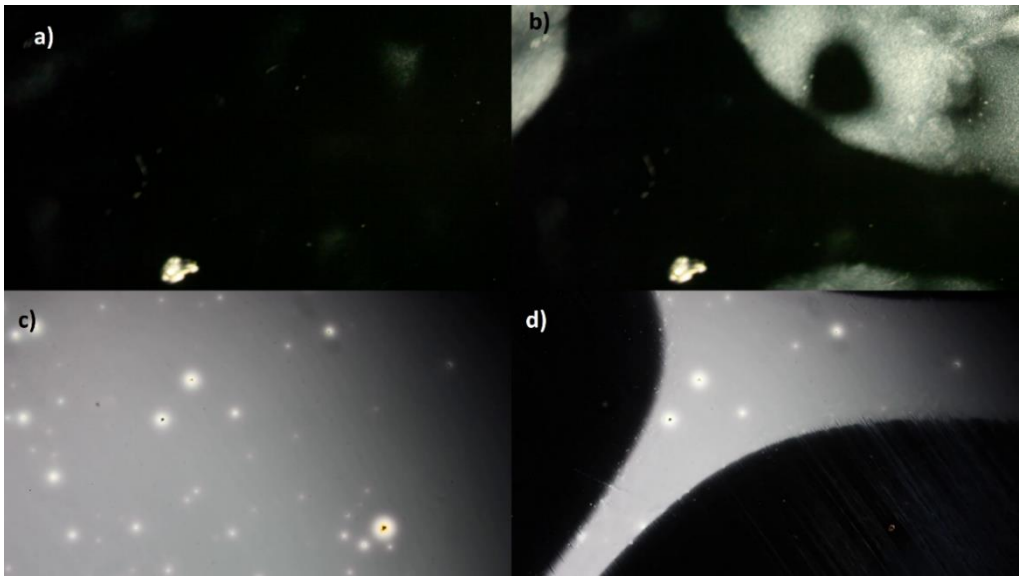

Figure 31: Image showing three distinct transition regions which correspond to the three different corona tips. a) shows the homeotropic detector in the off state. b) shows the homeotropic detector in the on state, with independent regions which have undergone transition in the top right, top left and the bottom right. c) shows the hybrid detector in the off state. d) shows the hybrid detector in the on state, with independent regions which have undergone transition in the top right, bottom right and the center left.

This test had several difficulties. Since the electric field, and hence the necessary voltage for a corona discharge event to take place, is dependent on both the distance from the grounded plate and the curvature of the conductor, all tips needed to be sharpened nearly identically, and the three source needed to be equidistant from the ITO to a high degree of accuracy. This was done through a trial and error process.

5.2 Electrons at the Surface

To confirm that electrons are indeed reaching the slide, the current through the liquid crystal layer was measured. The corona source was placed over the samples, and the tip and two grids were connected to three independent high voltage power supplies. The sample was grounded through an electrometer which measured the current through the sample. A protection circuit was constructed, as shown in figure 32, which prevented arcing events from damaging the electrometer.

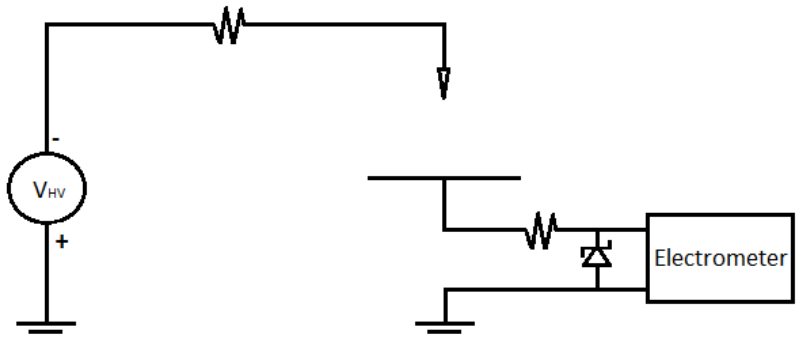

Figure 32: Circuit made to protect the electrometer. In the event of arcing, the Zener diode acts as a shunt, which protects the delicate circuitry of the electrometer.

When in normal operation, without arcing, the electrometer measures the current flowing from the sample to ground. The measured current is equal to the current being reaching the top surface of the liquid crystal, minus some amount of charge which is accumulating on the surface. As an initial test, the cells were imaged and the current through the device was recorded. The top grid

was held at -800 V and the bottom grid was held at -500 V. The voltage on the tip was increased in steps of 100 V. This is shown in figure 33.

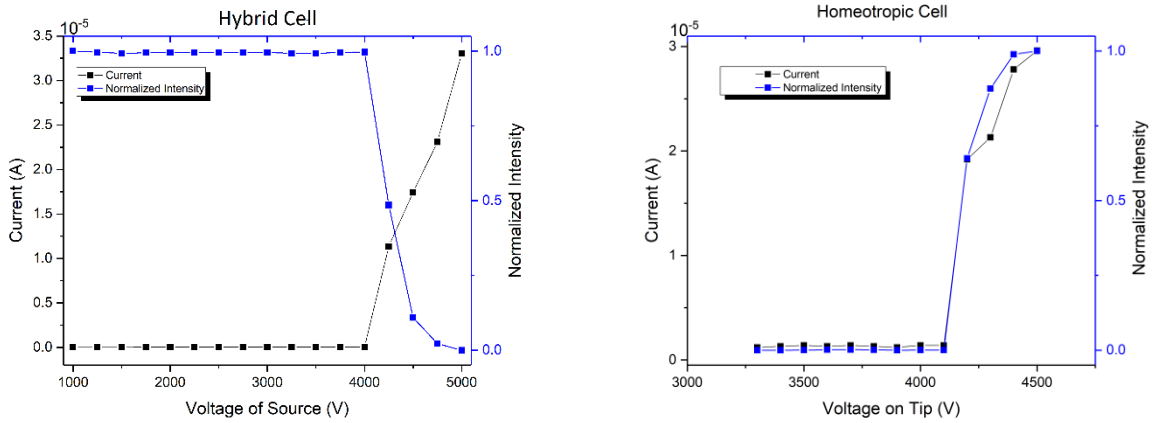

Figure 33: Graphs showing the intensity and current through a hybrid (left) and a homeotropic (right) sample as a function of the voltage applied to the corona source.

Both of these graphs show that the layers remain approximately unchanged, until a current begins to flow through them.

5.3 Control of Current Reaching Liquid Crystal

To progress with these tests, it was necessary to find a method with which the current reaching the liquid crystal layer could be effectively controlled and easily switched on and off. A corona source was designed to have two grids, as is described in section 3.4. The tip was held at a large negative voltage, and the top grid was kept at a smaller negative voltage. The bottom grid had a variable voltage applied, which was intended to allow for control over the electrons reaching the bottom surface, and operated much like a triode amplifier. To be able to quickly change polarity of the voltage applied to the bottom grid, a square wave supplied by a Keithly Arbitrary Waveform Generator was amplified using a Trek50/750 amplifier so that the magnitude of the applied voltage was in the range of hundreds of volts. By quickly changing the

magnitude of this voltage, or the polarity of the voltage, the number of electrons reaching the sample could rapidly be amplified or extinguished. The slew rate of the Trek amplifier is 150V/ms, so we can be confident that switching the magnitude of the voltage by 1000 V will take place in under 7 ms[1].

To show that this allowed for control over the current reaching the liquid crystal layers, the following experiment was performed. A hybrid aligned sample was prepared on an ITO plate. This was then grounded through the electrometer circuit as is described previously. This layer was then placed in the corona source apparatus. The tip of the corona source was held at -3300V, the top grid was held at -800V and the bottom grid had a variable voltage supplied by the Trek amplifier. The voltage on the bottom grid was then ramped from 500 V to -1000V, in steps of 100 V imaging the sample at each step. The current through the E7 layer was found at each step via the electrometer. This plot is shown in figure 34.

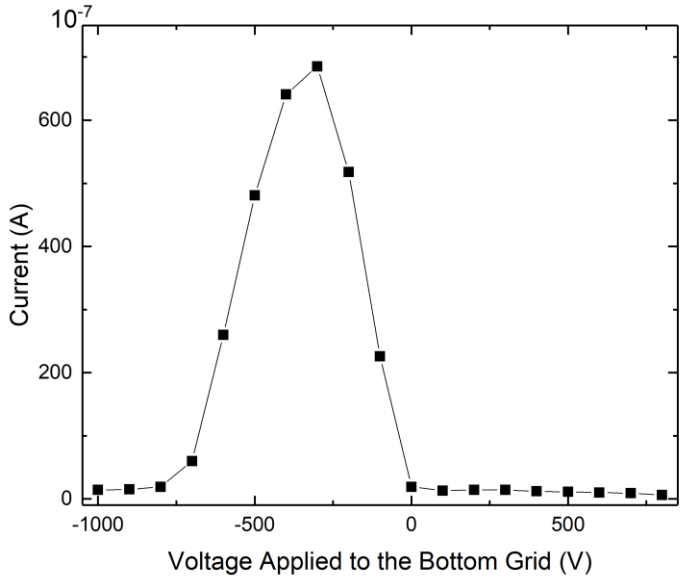

Figure 34: Graph showing the effectiveness of the bottom grid at quenching the electrons reaching the hybrid samples.

It is clear from this graph that current through the E7 layer substantially drops when the voltage applied to the bottom grid is much more negative than the voltage of the top grid. This is because the electrons which have reached the top grid are no longer accelerated toward the more negative bottom grid. The current also drops when the voltage on the bottom grid is a positive or a negative voltage with a small magnitude. This is because the electrons which have reached the positive bottom grid are no longer accelerated toward the grounded plate.

5.4 Initial Test to Determine Charge Density Deposited on the Layers

It is encouraging to see the transition in the liquid crystal layers correspond so closely to the measured current reaching the layers, but it would be best to have direct support for the proposed mechanism of transition. To determine the cause of the optical change in the layers, it is necessary to measure the voltage across the liquid crystal due to the electrons that are deposited on the layer. This cannot be measured directly, so it will need to be inferred from measurements that can be done. In this case, we will use the current to estimate of the magnitude of charge dispersed over the liquid crystal layer, and will use this to find the voltage across the layer. This is why it was necessary to determine the configuration of charges on the liquid crystal layer in section 3.7. This section will describe an experiment used to measure the charge established on the top surface of the liquid crystal, will establish an estimate of the voltage across the liquid crystal layer and then compare this with expected values.

To begin, two identically sized pieces of ITO were cleaned, and one was prepared with a hybrid E7 layer, following the procedure in section 3.1. Both the uncoated ITO slide and the slide having the E7 layer were placed under the corona source in turn, and the current through the layers was monitored via the electrometer circuit described in section 5.1.

During the experiment, the tip was held at -3600 V, the upper grid was kept at -800 V and the bottom grid was initially held at + 500 V. A square pulse was sent to the bottom grid, quickly changing the voltage from +500 V to -500 V, and the current was recorded as a function of time. The current as a function of time through both layers is plotted in figure 34.

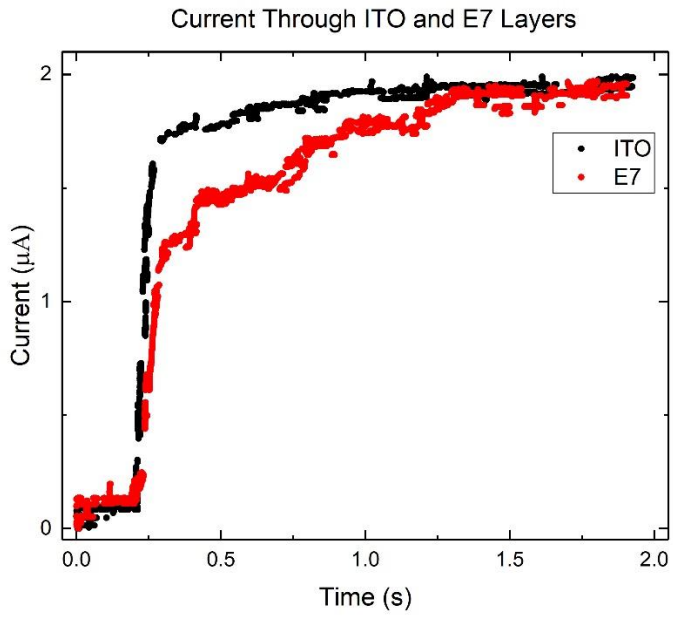

Figure 34: Current from corona source through plain ITO (black), and through ITO coated with a hybrid E7 layer (red).

By integrating the current through the ITO over time, we find the total charge which has passed through the ITO. By integrating the current measured from the E7 coated ITO slide, we find the total charge which has passed through the ITO plate beneath the E7 layer. Now, we will assume that the presence of the liquid crystal layer does not cause a significant change in the potential prior to the charge beginning to build up. Therefore, during these early times, the current reaching the surface of either the ITO or liquid crystal will be the same. In the case of the plain ITO slide, the current reaching the surface of the ITO sample is the current which we are measuring directly. This is not the case for the ITO coated with E7. The current reaching the

surface of the liquid-crystal-coated sample, first reaches the E7-air interface and then migrates to ground where it can be measured. Only the current which passes through the E7 layer and reaches the grounded ITO plate is measured. This means that, although the current reaching the liquid crystal surface and the plain ITO plate are approximately the same, the measured current may not be, as some of the charge may be accumulating on the liquid crystal layer. We can find an estimate for the charge on the surface of the liquid crystal using the measurement of the current through the E7 coated ITO plane and the plain ITO plate. The difference between these two currents is assumed to be the current which is accumulating on the liquid crystal layer. Integrating this over time, will give the total charge which has built up on the liquid crystal layer. The difference between the current through the plain ITO plate and the plate coated with E7 is shown in figure 35.

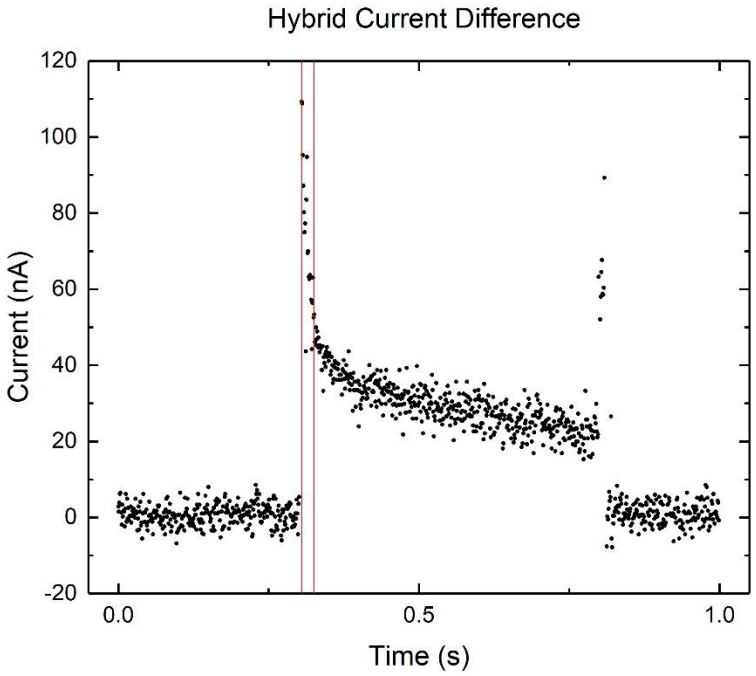

Figure 35: Difference between the current through the ITO and the ITO coated with E7. The vertical red lines signify the region which was integrated over.

We must now choose a time to integrate over. It was found that there was a delay of 20 ms between when the bottom grid changed polarity and when the liquid crystal layer began to change optically. This will be taken to be the time necessary to build up enough change to begin a significant transition. By integrating the above curve over the first 20 ms, we found that the charge which is deposited on the E7 is 14 nC. We have a model for how this charge is distributed, from our work in section 3.7. We are taking the functional form of the deposited charge density to be $Q(r,\theta) = Acos^5\left(arctan\left(\frac{r}{1\,mm}\right)\right)$. From the current measured above, we are able to determine the constant A. If we integrate the current density over the entire plate, we find the total current passing through this region. Doing this integral, we find

$$Q = \int_0^{\infty}\int_0^{2\pi} Acos^5\left(arctan\left(\frac{r'}{0.001}\right)\right)r'dr'd\theta' = 2.09 * 10^{-6}\,A$$

which we can equate with the measured charge of the hybrid layer sample to find the functional form of the charge distribution. We are able to see that

$$2.09 * 10^{-6}\,A = 14\,nC \rightarrow A = 6.7 * 10^{-3}C$$

The charge density on the liquid crystal layer is then taken to be

$$Q(r,\theta) = (6.7 * 10^{-3}C)cos^5\left(arctan\left(\frac{r}{0.001}\right)\right)$$

Now, having the charge density worked out, we are able to find the voltage across the layer. The voltage across the layer is found as

$$V(\vec{x}) = -\int_0^{h} z'\hat{z}\cdot\vec{E}(\vec{x})dz'$$

Where h is the thickness of the liquid crystal layer. We are then able to use this to find the potential as follows

$$V(\vec{x}) = \vec{E}(\vec{x}) \cdot \hat{z} = \frac{1}{4\pi\varepsilon_0\varepsilon_{lc}} \int_0^h \int_0^{2\pi} \int_0^{\infty} \frac{Q(r',\theta')}{|\vec{x} - \vec{x}'|^3} z' r' dr' d\theta' dz'$$

$$= \frac{A}{4\pi\varepsilon_0\varepsilon_{lc}} \int_0^h \int_0^{2\pi} \int_0^{\infty} \frac{cos^5\left(arctan\left(\frac{r'}{0.001}\right)\right)}{((r'cos\theta' - rcos\theta)^2 + (r'sin\theta' - rsin\theta)^2 + h^2)^{\frac{3}{2}}} z' r' dr' d\theta' dz'$$

$$= \frac{A}{4\pi\varepsilon_0\varepsilon_{lc}} \int_0^h \int_0^{2\pi} \int_0^{\infty} \frac{cos^5\left(arctan\left(\frac{r'}{0.001}\right)\right)}{((r'cos\theta' - r)^2 + (r'sin\theta')^2 + h^2)^{\frac{3}{2}}} z' r' dr' d\theta' dz'$$

Now, we are able to find the voltage across the layer at each point. First, it is useful to find at the voltage at r = 0, directly in the center of the transition region. If we take the dielectric constant of E7 to be $\varepsilon_{lc} = 11$, set r = 0 and numerically integrate we find that the voltage across the layer is $21V^2$. This is larger than necessary to cause a transition since, in a planar aligned sample, the known Freedericksz threshold voltage of E7 is 0.9 V_{rms}[3]. This does show that the voltage is approximately what would be expected, up to an order of magnitude.

It was observed that the radius of transition of the liquid crystal layers was approximately 2 mm. If we choose r = 2 mm and integrate, we find that the voltage predicted voltage across the layer is 0.4 V. It is certainly believable that the transition would be much less pronounced at this radius.

Chapter 6

Experimental Work with Gas Electron Multiplier

With proof of concept finished and the liquid crystal layers having been tested, work on the project shifted to the development of the gas electron multiplier. The gas electron multiplier will allow for similar measurements as was done in the previous sections, however, it should yield much cleaner data. This section will describe the beginning work on the gas electron multiplier.

6.1 Measuring the Gain of the Gas Electron Multiplier

As an initial test, it was important to determine whether the gas electron multiplier multiplied electrons as would be expected. In this initial test, the top grid was held at -2000V and the center grid was held at -200V. The bottom grid was grounded, and was monitored using an amplifier and an oscilloscope. Since the mesh is sufficiently finely spaced, any electron showers generated in the region above will be deposited on the bottom grid, and can be measured through the amplifier.

It was noticed that there were many negative pulses which are much larger than the background noise. These increased in frequency and amplitude as the electric field between the top and center grid was increased, and were extinguished when the electric field in this region was turned off. A typical waveform of one of these pulses is shown in figure 36.

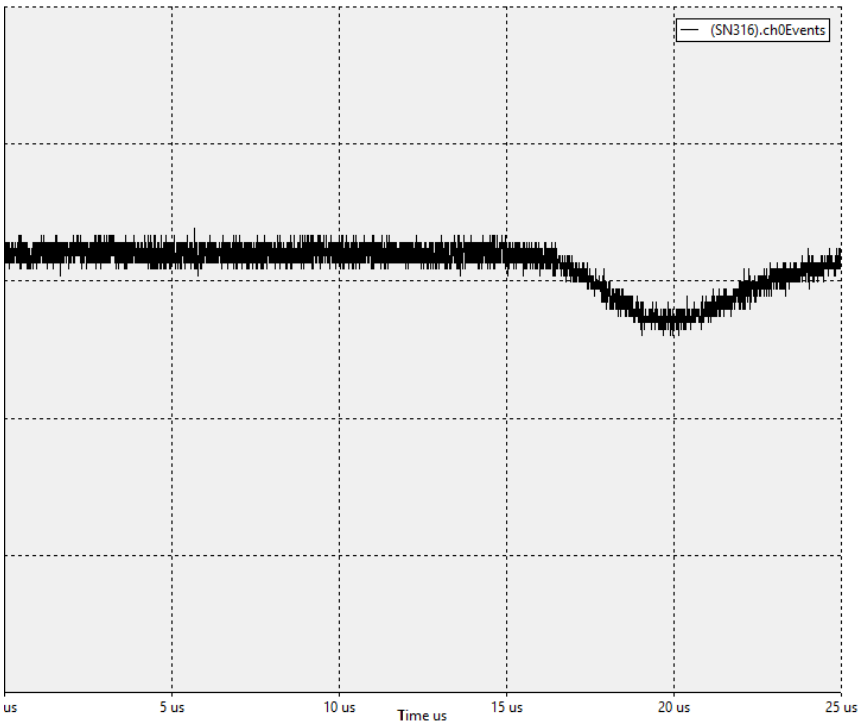

Figure 36: Typical pulse observed from the gas electron multiplier. The vertical axis is in units of 100 mV/div, with an arbitrary DC offset.

The trigger of the scope was set so that only pulses having at least half of the maximum allowed amplitude were counted. The scope was set to count the number of pulses per second. It was expected that the fewest number of pulses would be observed when the americium sample was not in place, and when the region was filled with air. It was also expected that the most pulses would be seen when the americium sample was in place, and when the chamber was flooded with argon. Each possible arrangement was tried, and the results are displayed in table 5.

Table 5: Results of initial test with gas electron multiplier.

	With Air	**With Argon**
Without Americium	< 10 Hz	80 ± 10 Hz
With Americium	~ 10 Hz	110 ± 20 Hz

The scope allowed the frequency to be as low as 10 Hz, meaning that we were unable to put error bars on the measurements done in air. This initial test agrees with expectation, and shows that the chamber is functioning as expected, at least qualitatively. This will be quantified in the next section

6.2. Counts Per Second of the Gas Electron Multiplier

It is known that increasing the voltage difference between the plates will increase the gain exponentially[1]. To test if the gas electron multiplier is behaving appropriately, we used an Ortec model 441 ratemeter to count the number of pulses as a function of the applied electric field. The ratemeter counts the pulses per second with an amplitude larger than some threshold voltage set by the manufacturer. The time constant of the ratemeter was set sufficiently high so that the fluctuations observed in the previous measurement were averaged out. The voltage on both the top and center grid were varied and the rate of counts was recorded. The results of this test is shown in figure 37.

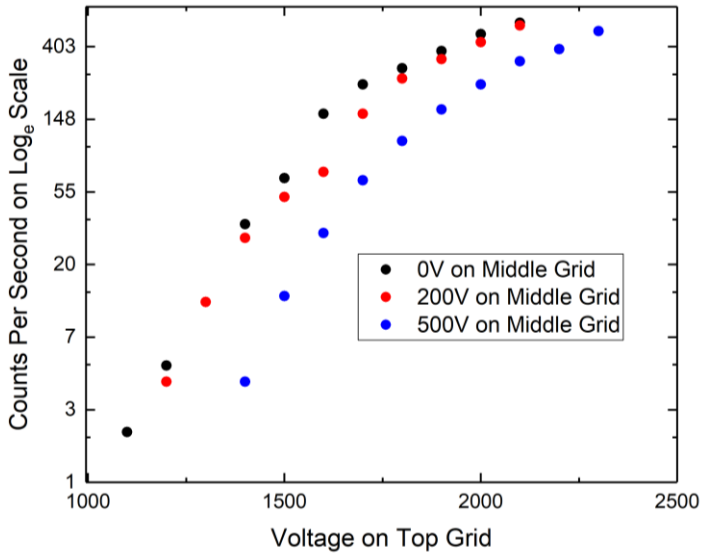

Figure 37: The number of counts versus the applied electric field between the top and middle grid. The voltage applied to the middle grid was stepped up to increase the voltage between the middle and bottom grid for several different runs.

This test shows that the gas electron multiplier is behaving approximately correctly, although there is a bit of variation from linear behavior near the edge of the upper measured range.

Chapter 7

Discussion

7.1 Potential Future Work

There is still much work to be done to fully develop the layers for use as an electron detector. There are several more variables that may be optimized, and opportunities to improve on the work already done.

The next most immediate step will be to measure the voltage due to the charge density across the homeotropic ZLI-2806 layers. This test will yield more interesting information than the test with the E7 layers, since the homeotropic layers will have a Freedericksz transition, allowing for an exact voltage threshold for transition. This measurement has already been done for a homeotropic layer fabricated using a different method than described in section 3.2. It was later found, however, that the liquid crystal layers fabricated in this way were not of uniform thickness throughout, so the measurements may not have been reliable.

Another extremely important step in the experiment will be fabricating a stable homeotropic liquid crystal layer. A useable layer will be polymerizable, will wet the polyimide in the long term and will not be damaged when used exposed to electrons. Several methods were developed which were able to achieve some combination of two of these three things, but none was found which was able to do all three. This is an important experimental hurdle which will need to be overcome.

Due to time constraints, it was not possible to test the liquid crystal layers under the gas electron multiplier. The next step will be measuring the gain of the gas electron multiplier carefully, so that a well-established amount of charge is deposited on the layer each time. Testing

the layers under the gas electron multiplier is an important step in demonstrating the effectiveness of the liquid crystal layers at detecting charged particles. The gas electron multiplier will be able to deliver a well-defined quantity of charge over a smaller area than the corona source. The experimental setup for the gain tests is nearly finished, and these final tests should be completed shortly.

7.2 Acknowledgements

I would like to thank Dr. Charles Rosenblatt, my primary research adviser, for his continual help from the outset of the project. I would also like to acknowledge Dr. Rolfe Petschek for his involvement with the inception of the project and his input throughout its development. I would like to thank Dr. Ben Monreal for his part in the inception of the project and his continued experimental and theoretical input in the project.

7.3 Concluding Remarks

There are many different types of charged particle detectors currently in use. Each type of detector has its own important properties which make it useful in specific experimental applications. The invention of a novel detector brings with it the possibility of new and exciting applications. Until the liquid crystal detector is developed and completely characterized, how competitive it will be in comparison to other detectors is unknown. This project has worked to develop liquid crystal films that may be used as a charged particle detector. We expect that our liquid crystal detector will allow for the detection of charged particles with a spatial resolution appropriate for a variety of application, while being much more cost effective than current detectors. This project is an exciting new application in the well-established field of liquid crystals.

References

Chapter 2

1) “History and Properties of Liquid Crystals: An Entirely New Phase of Matter”, https://www.nobelprize.org/educational/physics/liquid_crystals/history/.

2) B. Bahadur, “Liquid Crystals – Applications and Uses” (Litton Systems Canada, 1990), Vol. 1.

3) Sigma Aldrich,https://www.sigmaaldrich.com/catalog/product/aldrich/328510?lang=en&region=US, Accessed February 22, 2018.

4) P.G. de Gennes and J. Prost. “The Physics of Liquid Crystals.” (Oxford Science Publications, Oxford, 2003), 2nd Edition. pg 133.

5) Collings, Peter J., and Michael Hird. “Introduction to liquid crystals: chemistry and physics.” *CRC Press*, 1997.

6)S. Chandrasekhar. “Liquid Crystals” (Cambridge University Press, Cambridge, 1977).First Edition. Pg 59-61, 112-115.

7) Čopar, Simon. "Topology and geometry of nematic braids." *Physics Reports* 538, no. 1 (2014): 1-37.

8) Crawford, Gregory Philip, and Slobodan Zumer, eds. “Liquid crystals in complex geometries: formed by polymer and porous networks.” *CRC Press*, 1996.

9) V. Jayalakshmi, G. Hegde, G. G. Nair and S. K. Prasad, *Phys. Chem. Chem. Phys.*, 2009, 11, 6450–6454.

10)A. Amirsadeghi, J. Lee, “Supplemental Information” *Appl. Surf. Sci*., 2011, 258(3):1272-1278

11) Ciba Specialty Chemicals Inc. “Ciba Irgacure 651 Photoinitiator”. Edition 4.9.2001, Basle.

12) Chang, J-S., Phil A. Lawless, and Toshiaki Yamamoto. "Corona discharge processes." *IEEE Transactions on plasma science* 19, no. 6 (1991): 1152-1166.

13) Hong, Alice (2000). "Dielectric Strength of Air". *The Physics Factbook*.

14) *Kuffel, E.; Zaengl, W. S.; Kuffel, J. (2004).* “High Voltage Engineering Fundamentals (2nd ed.)”. *Butterworth-Heinemann. ISBN 0-7506-3634-3.*

15) Townsend, John Sealy. “Electricity in gases.” *Рипол Классик,* 1915.

16) M. Juiaihi. “Synthesis of metallic oxide nanoballs via submerged glow-discharge plasma and their photocatalytic effect”, 2015.

17) Sauli, Fabio. "GEM: A new concept for electron amplification in gas detectors." *Nuclear Instruments and Methods in Physics Research Section A: Accelerators, Spectrometers, Detectors and Associated Equipment* 386, no. 2-3 (1997): 531-534.

Chapter 3

1) Cooper J. “Compositional analysis of Merck E7 liquid crystals intermediates using UltraPerformance Convergence Chromatography (UPC2) with PDA detection.” *Waters*.

2) I. Gharbi. “Report of Oily streaks skeleton into a nematic phase”. Internal Report from 2015.

3) Jackson, John David. "Classical electrodynamics." (1999): p. 47-50.

4) UNAM database, private communication, www.lxcat.net, retrieved on March 20, 2018.

5) Yachi, S., Y. Kitamura, K. Kitamori, and H. Tagashira. "A multi-term Boltzmann equation analysis of electron swarms in gases." *Journal of Physics D: Applied Physics* 21, no. 6 (1988): 914.

6) Dutton database, www.lxcat.net, retrieved on March 20, 2018.

7) M. Rabie and C.M. Franck, "METHES: A Monte Carlo collision code for the simulation of electron transport in low temperature plasmas”, *Comput. Phys. Comm.,* 203 (2016), pp. 268-277 as well as M. Rabie and C.M. Franck, METHES code, downloaded from www.lxcat.net/download/METHES, 2015.

8) Zimmer, Carl (3 October 2013). "Earth's Oxygen: A Mystery Easy to Take for Granted". *New York Times*. Retrieved 3 October 2013.

9) Robledo-Martinez, A. "Characteristics of DC corona discharge in humid, reduced-density air." *Journal of Electrostatics* 29, no. 2 (1993): 101-111.

Chapter 4

1) Wu, Shin-Tson, Uzi Efron, and LaVerne D. Hess. "Birefringence measurements of liquid crystals." *Applied optics*23, no. 21 (1984): 3911-3915.

2) Bahadur, B., R. K. Sarna, and V. G. Bhide. "Refractive indices, density and order parameter of some technologically important liquid crystalline mixtures." *Molecular Crystals and Liquid Crystals* 72, no. 5-6 (1982): 139-145.

3) Trivedi et al. SI Text 10.1073/pnas.1119118109

Chapter 5

1) TREK Incorparated. “Operator’s Manual Model 50/750 High Voltage Amplifier” p. 2A

2) Viciosa, M. T., A. M. Nunes, A. Fernandes, P. L. Almeida, M. H. Godinho, and M. D. Dionísio. "Dielectric studies of the nematic mixture E7 on a hydroxypropylcellulose substrate." *Liquid crystals* 29, no. 3 (2002): 429-441.

3) Brown, C. V., and N. J. Mottram. "Influence of flexoelectricity above the nematic Fréedericksz transition." *Physical Review E*68, no. 3 (2003): 031702.

Chapter 6

1) Sauli, Fabio. "GEM: A new concept for electron amplification in gas detectors." *Nuclear Instruments and Methods in Physics Research Section A: Accelerators, Spectrometers, Detectors and Associated Equipment* 386, no. 2-3 (1997): 531-534.